Monthly Notices
of the
ROYAL ASTRONOMICAL SOCIETY

MNRAS **441,** 1243–1259 (2014) doi:10.1093/mnras/stu627

The effect of bars on the $M_\bullet - \sigma_e$ relation: offset, scatter and residuals correlations

Markus Hartmann,[1,2⋆] Victor P. Debattista,[2⋆] David R. Cole,[2⋆] Monica Valluri,[3⋆] Lawrence M. Widrow[4⋆] and Juntai Shen[5⋆]

[1]*Astronomisches Rechen-Institut, Zentrum für Astronomie der Universität Heidelberg (ZAH), Mönchhofstr. 12-14, D-69120 Heidelberg, Germany*
[2]*Jeremiah Horrocks Institute, University of Central Lancashire, Preston PR1 2HE, UK*
[3]*Department of Astronomy, University of Michigan, 500 Church St, Ann Arbor, MI 48109, USA*
[4]*Department of Physics, Engineering Physics, and Astronomy, Queen's University, 99 University Avenue, Kingston, ON K7L 3N6, Canada*
[5]*Shanghai Astronomical Observatory, 80 Nandan Road, Shanghai 200030, China*

Accepted 2014 March 24. Received 2014 March 16; in original form 2013 August 18

ABSTRACT

We analyse a set of collisionless disc galaxy simulations to study the consequences of bar formation and evolution on the $M_\bullet - \sigma_e$ relation of supermassive black holes (SMBHs). The redistribution of angular momentum driven by bars leads to a mass increase within the central region, raising the velocity dispersion of the bulge, σ_e, on average by ∼12 per cent and as much as ∼20 per cent. If a disc galaxy with an SMBH satisfying the $M_\bullet - \sigma_e$ relation forms a bar, and the SMBH does not grow in the process, then the increase in σ_e moves the galaxy off the $M_\bullet - \sigma_e$ relation. We explore various effects that can affect this result including contamination from the disc and anisotropy. The displacement from the $M_\bullet - \sigma_e$ relation for individual model barred galaxies correlates with both the bulge-to-total stellar mass ratio, $M(\mathrm{B})/M(\mathrm{B}+\mathrm{D})$, and the 2D anisotropy, $\beta_\phi(\mathrm{B}+\mathrm{D})$, both measured within the effective radius of the bulge. Overall, this process leads to an $M_\bullet - \sigma_e$ for barred galaxies offset from that of unbarred galaxies, as well as an increase in its scatter. We assemble samples of observed unbarred and barred galaxies with classical bulges and find tentative hints of an offset between the two consistent with the predicted. Including all barred galaxies, rather than just those with a classical bulge, leads to a significantly larger offset, which is mostly driven by the significantly larger offset of pseudo bulges.

Key words: black hole physics – galaxies: bulges – galaxies: evolution – galaxies: kinematics and dynamics – galaxies: nuclei – galaxies: structure.

1 INTRODUCTION

One of the most striking results to emerge from *Hubble Space Telescope* (*HST*) observations is that essentially every galaxy with a significant stellar spheroid contains a supermassive black hole (SMBH) whose mass is correlated with properties of the host galaxy. For instance the masses of SMBHs, $M_\bullet$, are found to correlate with the bulge luminosity, $L_{\rm bul}$ (Kormendy & Richstone 1995; McLure & Dunlop 2002; Marconi & Hunt 2003; Graham 2007; Gültekin et al. 2009; Sani et al. 2011; McConnell et al. 2011; Beifiori et al. 2012; Graham & Scott 2013), with the bulge mass, $M_{\rm bul}$ (Magorrian et al. 1998; Marconi & Hunt 2003; Häring & Rix 2004; Sani et al. 2011; Beifiori et al. 2012; Graham 2012), the bulge velocity dispersion, $\sigma_{\rm e}$ (Ferrarese & Merritt 2000; Gebhardt et al. 2000; Merritt & Ferrarese 2001; Tremaine et al. 2002; Ferrarese & Ford 2005; Gültekin et al. 2009; Graham et al. 2011; McConnell et al. 2011; Beifiori et al. 2012), with the mass of the galaxy (either stellar or total), $M_{\rm gal}$ (Ferrarese 2002; Baes et al. 2003; Kormendy & Bender 2011; Volonteri, Natarajan & Gültekin 2011; Beifiori et al. 2012), with the Sérsic index of the surface brightness profile, n (Graham et al. 2001; Graham & Driver 2007), with the spiral pitch angle (Seigar et al. 2008; Berrier et al. 2013), with the number of globular clusters (Burkert & Tremaine 2010; Harris & Harris 2011; Rhode 2012), with the globular cluster system velocity dispersion (Sadoun & Colin 2012; Pota et al. 2013) and with the inner core radius, r_γ (Lauer et al. 2007; Kormendy & Bender 2009). Amongst these, the $M_\bullet - \sigma_e$ relation with the form $\log(M_\bullet/\mathrm{M}_\odot) = \alpha + \beta \log(\sigma/200\,\mathrm{km\,s^{-1}})$ (Ferrarese & Merritt 2000; Gebhardt et al. 2000) is one of the tightest (Gebhardt et al.

⋆ E-mail: hartmann@ari.uni-heidelberg.de (MH); vpdebattista@gmail.com (VPD); drdrcole@gmail.com (DRC); mvalluri@umich.edu (MV); widrow@astro.queensu.ca (LMW); jshen@shao.ac.cn (JS)

Table 1. Published values for the zero-point, α, slope, β, and scatter of the $M_\bullet - \sigma_e$ relation from a number of studies. For the Graham et al. (2011) and McConnell & Ma (2013) studies, we also present the results found for different galaxy type.

	α	β	ϵ_0
Gebhardt et al. (2000)	8.08 ± 0.06	3.75 ± 0.3	0.3
Merritt & Ferrarese (2001)	8.11 ± 0.11	4.72 ± 0.36	0.35
Tremaine et al. (2002)	8.13 ± 0.06	4.02 ± 0.32	0.33
Ferrarese & Ford (2005)	8.22 ± 0.06	4.86 ± 0.43	0.34
Gültekin et al. (2009)	8.12 ± 0.08	4.24 ± 0.41	0.44
Graham et al. (2011)	8.13 ± 0.05	5.13 ± 0.34	0.43
Beifiori et al. (2012)	8.19 ± 0.07	4.17 ± 0.32	0.41
McConnell & Ma (2013)	8.32 ± 0.05	5.64 ± 0.32	0.38
Graham et al. (2011)			
Barred	7.80 ± 0.10	4.34 ± 0.56	0.36
Unbarred	8.25 ± 0.06	4.57 ± 0.35	0.37
Elliptical	8.27 ± 0.06	4.43 ± 0.57	0.34
McConnell & Ma (2013)			
Early type	8.39 ± 0.06	5.20 ± 0.36	
Late type	8.07 ± 0.21	5.06 ± 1.16	

2003; Marconi & Hunt 2003; Gültekin et al. 2009). The intrinsic scatter in this relation, ϵ_0 has increased in recent studies (see Table 1). Here, β is the slope and α is the zero-point of the relation. Measurements of β have produced a variety of different results (see Table 1). Early estimates varied from 3.75 ± 0.3 (Gebhardt et al. 2000) to 4.8 ± 0.5 (Ferrarese & Merritt 2000). More recently, Gültekin et al. (2009) found $\beta = 4.24 \pm 0.41$, whereas McConnell & Ma (2013) found $\beta = 5.64 \pm 0.32$ and Graham et al. (2011) found $\beta = 5.13 \pm 0.34$, demonstrating that the slope of the relation remains imperfectly determined. Sources of this variation are the uncertainty in the data (see for example section 5 of McConnell & Ma 2013), different linear regression techniques (e.g. Graham et al. 2011) and different slopes in different galaxy types. McConnell & Ma (2013) find different values of α and β for early- and late-type galaxies (see Table 1) while Graham et al. (2011) and Graham & Scott (2013) find different values of α and β for barred and unbarred galaxies. Graham & Scott (2013) find a different zero-point but common slope for barred and unbarred galaxies; some of the difference in slope may therefore even be due just to a difference in the fraction of barred galaxies in different samples. Such differences must be explained by any model explaining the link between SMBHs and their hosts.

SMBH scaling relations suggest that there is a connection between the growth of the SMBH and the bulge. However, the causal basis of these scaling relations is still not fully understood. Does the presence of an SMBH govern the bulge's growth or is the growth of the SMBH determined by the bulge it resides in? The vast energy available from an accreting SMBH during its phase as an active galactic nucleus (AGN) can couple the SMBH to its host, since only a small fraction of this energy is needed to alter the temperature and structure of the surrounding interstellar medium (Silk & Rees 1998; King 2003; Wyithe & Loeb 2003; Di Matteo, Springel & Hernquist 2005; Murray, Quataert & Thompson 2005; Sazonov et al. 2005; Younger et al. 2008; Booth & Schaye 2009; Power et al. 2011). Alternatively, the $M_\bullet - \sigma_e$ relation could merely be a consequence of the merger history in a hierarchical universe (Adams, Graff & Richstone 2001; Adams et al. 2003; Volonteri & Natarajan 2009; Shankar et al. 2012), as could be scaling relations with galaxy or bulge mass (Peng 2007; Jahnke & Macciò 2011) and the tightening of the relations with galaxy mass (Hirschmann et al. 2010).

Graham (2008b) and Graham & Li (2009) found that SMBHs in barred galaxies have an offset from the $M_\bullet - \sigma_e$ relation of elliptical galaxies (see also Graham et al. 2011; Graham & Scott 2013). In addition, excluding barred galaxies from the $M_\bullet - \sigma_e$ relation reduces the scatter ϵ_0 from 0.47 to 0.41 (Graham & Li 2009). Both Hu (2008) and Gadotti & Kauffmann (2009) point out that the presence of bars could be responsible for the difference in these $M_\bullet - \sigma_e$ relations. Graham (2008a) and Graham & Li (2009) obtained an $M_\bullet - \sigma_e$ relation for unbarred galaxies and Graham et al. (2011) showed that barred galaxies have an offset of ∼0.5 dex from this relation. On the other hand, amongst active galaxies with $M_\bullet < 2 \times 10^6$ $M_\odot$, Xiao et al. (2011) found no significant offset of barred galaxies relative to the $M_\bullet - \sigma_e$ relation of unbarred galaxies. Likewise, in a sample of galaxies with active nuclei for which they obtained upper limits on $M_\bullet$, Beifiori et al. (2009) found no systematic difference between barred and unbarred galaxies.

Bars, either weak or strong, are present in ∼65 per cent of local luminous disc galaxies (Knapen 1999; Eskridge et al. 2000; Nair & Abraham 2010; Masters et al. 2011). The fraction of *strongly* barred galaxies rises from ∼20 per cent at $z \sim 1$ to ∼30 per cent at $z = 0$ (Elmegreen, Elmegreen & Hirst 2004; Jogee et al. 2004; Sheth et al. 2008; Skibba et al. 2012). Thus, bars have had a long time to drive evolution in disc galaxies (Courteau, de Jong & Broeils 1996; Debattista et al. 2004, 2006; Kormendy & Kennicutt 2004; Jogee, Scoville & Kenney 2005). Bars lead to a redistribution of angular momentum and an increase in the central mass density (Hohl 1971). Therefore, they provide a possible mechanism for fuelling central starbursts and AGN activity (Simkin, Su & Schwarz 1980; Athanassoula 1992; Shlosman, Frank & Begelman 1989; Jogee, Scoville & Kenney 2005; Schawinski et al. 2011; Hicks et al. 2013). While near-infrared surveys find no difference in the fraction of barred galaxies between active and non-active galaxies (McLeod & Rieke 1995; Mulchaey & Regan 1997; Cisternas et al. 2013), this could be due to the vastly disparate time-scales involved, with AGN having an active phase of the order of 10^6 yr compared to the ∼100 × longer quiescent phase (Shabala et al. 2008).

Besides fuelling the SMBH, bars may affect a galaxy's position on the $M_\bullet - \sigma_e$ relation in other ways. Graham et al. (2011) proposed that several bar driven effects can cause offsets in the $M_\bullet - \sigma_e$ relation, including velocity anisotropy, and the increase in σ_e due to mass inflows, and buckling. Bars can also lead to the growth of pseudo-bulges by driving gas to the centre to fuel star formation (Kormendy & Kennicutt 2004), changing σ_e.

Another way in which bars can change the location of a galaxy on the $M_\bullet - \sigma_e$ relation is by transferring angular momentum outwards (Lynden-Bell & Kalnajs 1972; Tremaine & Weinberg 1984; Debattista & Sellwood 2000; Athanassoula 2002, 2003; Sellwood 2006; Berentzen et al. 2007), increasing the central density of the disc and raising the velocity dispersion of the bulge (Debattista et al. 2005; Brown et al. 2013; Debattista, Kazantzidis & van den Bosch 2013). This paper explores the effect of bar evolution on the $M_\bullet - \sigma_e$ relation of classical bulges, under the assumption that galaxies form without a bar, but with an SMBH that satisfies the $M_\bullet - \sigma_e$ relation. The bar then forms via gravitational instabilities in the disc. We show, using collisionless simulations, that as a result of angular momentum redistribution, such an SMBH ends up offset from the $M_\bullet - \sigma_e$ relation. In a companion paper, Brown et al. (2013) examine the effect of the growth of an SMBH on the nuclear stellar kinematics in both pure disc systems, and in systems composed of a disc and spheroidal bulge. They show that the presence of a bar

enhances the effect that the growth of an SMBH has on the stellar σ_e. Their simulations show that the growth of an SMBH after the formation of a bar also causes an offset in σ_e, but one that is smaller ($\sim$7 per cent) than that resulting from the formation and evolution of a bar. Thus, the current paper and the Brown et al. (2013) paper show that regardless of whether the SMBH exists prior to bar formation or whether it grows after bar formation (with reality being somewhere in between these two extremes), barred galaxies will have larger values of σ_e than unbarred galaxies with the same $M_\bullet$.

The paper is organized as follows: In Section 2, we describe the simulations. In Section 3, we study what effect bar formation and evolution have on the bulge and disc and how this might affect the $M_\bullet - \sigma_e$ relation. We discuss the consequences of bar evolution for the $M_\bullet - \sigma_e$ relation in Section 4 and compare our results with the observed $M_\bullet - \sigma_e$ relations of classical bulges in unbarred and barred galaxies. Section 6 sums up our findings.

2 SIMULATIONS

We use the set of 25 simulations from Widrow, Pym & Dubinski (2008, hereafter W08), which represents the evolution of a Milky Way-like galaxy from idealized initial conditions. The advantage of using these simulations (aside from their high-quality setup) is that they provide a range of possible evolutionary paths for at least one galaxy. By restricting ourselves to models for a single galaxy we underestimate the expected scatter in the evolution. Note that since collisionless simulations can be rescaled in mass, size and velocity subject to the condition $G = 1$, where G is the gravitational constant, our results can be applied to a fairly broad set of galaxy mass. Below we describe in brief the setup of the simulations and refer the reader to W08 for a more detailed discussion. These simulations are all collisionless, therefore here we are modelling just the gravitational effects of bar evolution; we discuss the implications of gas at the end of this paper. Simulations including gas will be presented elsewhere.

2.1 Galaxy models

The initial conditions for the simulations are N-body realisations of axisymmetric galaxy models that consist of a disc, a bulge and a dark matter halo. The distribution function for the composite system is

$$f(E,\, L_z,\, E_z) = f_{\rm d}(E,\, L_z,\, E_z) + f_{\rm b}(E) + f_{\rm h}(E), \tag{1}$$

where the energy E and the angular momentum about the symmetry axis L_z are exact integrals of motion and E_z is an approximate third integral corresponding to the vertical energy of stars in the disc (Kuijken & Dubinski 1995; Widrow & Dubinski 2005). Since E_z is very nearly conserved for orbits that are not far from circular, the initial system will be close to equilibrium so long as the disc is relatively 'cold', a condition met for the models considered in this paper.

The distribution function for the disc is constructed to yield the density distribution (Kuijken & Dubinski 1995)

$$\rho_{\rm d}(R, z) = \frac{M_{\rm d}}{2\pi R_{\rm d}^2}\, {\rm e}^{-R/R_{\rm d}}\, {\rm sech}^2(z/z_{\rm d})\, {\rm erfc}\left(\frac{r - R_{\rm t}}{2^{1/2}\delta R_{\rm t}}\right), \tag{2}$$

where R and z are the usual cylindrical coordinates, r the spherical radius, $R_{\rm d}$ the scalelength, $z_{\rm d}$ the scaleheight and $M_{\rm d}$ the total mass of the disc. The disc is truncated at radius $R_{\rm t} = 10R_{\rm d}$ with a truncation sharpness of $\delta R_{\rm t} = 1$ kpc. The distribution function is constructed so that the radial dispersion profile is exponential $\sigma_{\rm R}^2(R) = \sigma_{\rm R0}^2 \exp(-R/R_{\rm d})$, where $\sigma_{\rm R}$ is the radial velocity dispersion in cylindrical coordinates.

The bulge and halo distribution functions are designed so that their respective density profiles approximate the user-specified functions $\tilde{\rho}_{\rm b}$ and $\tilde{\rho}_{\rm h}$. For the bulge, we assume a 'target' density profile

$$\tilde{\rho}_{\rm b}(r) = \rho_{\rm b}\left(\frac{r}{R_{\rm eff}}\right)^{-p} {\rm e}^{-b(r/R_{\rm eff})^{1/n}}, \tag{3}$$

which yields, on projection, the Sérsic law with $p = 1 - 0.6097/n + 0.055\,63/n^2$ (Prugniel & Simien 1997; Terzić & Graham 2005), where n is the Sérsic index and $\rho_{\rm b}$ is the central surface density. The constant b is adjusted so that $R_{\rm eff}$ contains half of the total projected mass of the bulge. These models use

$$\sigma_{\rm b} \equiv \left(4\pi n b^{n(p-2)} \Gamma(n(2-p))\, R_{\rm eff}^2 \rho_{\rm b}\right)^{1/2} \tag{4}$$

rather than $\rho_{\rm b}$ to parametrize the overall density scale of the bulge models, where Γ is the gamma function.

The target halo density profile is

$$\tilde{\rho}_{\rm halo}(r) = \frac{2^{2-\gamma}\sigma_{\rm h}^2}{4\pi a_{\rm h}^2} \frac{1}{(r/a_{\rm h})^{\gamma}\,(1 + r/a_{\rm h})^{3-\gamma}}\, C(r; r_{\rm h}, \delta r_{\rm h}), \tag{5}$$

where $\gamma = 1$ is the central cusp strength, $a_{\rm h}$ is the scalelength and $C(r;\, r_{\rm h},\, \delta r_{\rm h})$ is a truncation function that decreases smoothly from unity to zero at $r \simeq r_{\rm h}$ within a radial range $\delta r_{\rm h}$. The models considered here assume $r_{\rm h} = 100$ kpc and $\delta r_{\rm h} = 5$ kpc and use the function $C(r; r_{\rm h}, \delta r_{\rm h}) = \frac{1}{2}{\rm erfc}((r - r_{\rm h})/\sqrt{2}\delta r_{\rm h})$.

The bulge and halo distribution functions, which, by assumption, depend only on the energy, are found via an inverse Abel transform (Binney & Tremaine 2008). Since this method assumes spherical symmetry, we first calculate an approximate spherically averaged total potential

$$\tilde{\Psi}_{\rm tot} = \tilde{\Psi}_{\rm d} + \tilde{\Psi}_{\rm b} + \tilde{\Psi}_{\rm h}, \tag{6}$$

where $\tilde{\Psi}_{\rm d}$ is the monopole term of a spherical harmonic expansion for the disc and $\tilde{\Psi}_{\rm b,h}$ are calculated from $\tilde{\rho}_{\rm b,h}$. We then evaluate

$$f_{\rm b,h}(E) = \frac{1}{\sqrt{8}\pi^2} \int_E^0 \frac{{\rm d}^2\tilde{\rho}_{\rm b,h}}{{\rm d}\tilde{\Psi}_{\rm tot}^2} \frac{{\rm d}\tilde{\Psi}_{\rm tot}}{\sqrt{\tilde{\Psi}_{\rm tot} - E}}. \tag{7}$$

Armed with the distribution functions for the three components, we solve Poisson's equation in *axisymmetry* using an iterative scheme and Legendre polynomial expansion (Kuijken & Dubinski 1995; Widrow & Dubinski 2005). Note that the bulge and halo are flattened slightly due to the influence of the disc potential.

2.2 Model parameters

The models described above were tailored to satisfy observational constraints for the Milky Way such as the inner and outer rotation curve, the local vertical force, the line-of-sight velocity dispersion towards Baade's window and the circular speed at the position of the Sun. A Bayesian/MCMC algorithm provided the probability distribution function (PDF) of Milky Way models over the model parameter space. Models from the PDF span a wide range of structural properties. For example, $M_{\rm d}$ varies in the range 2–7 $\times$ 10^{10} $M_\odot$, while $R_{\rm d}$ varies between 2.0 and 3.5 kpc.

The stability of a stellar disc is determined by the Toomre-Q and swing amplification parameter X:

$$Q = \frac{\sigma_{\rm R}\kappa}{3.36G\Sigma} \quad \text{and} \quad X \equiv \frac{\kappa^2 R}{2\pi G\Sigma m}, \tag{8}$$

Table 2. The sample of disc galaxy simulations used in this study. In the left-hand column, we list the run number and some of the initial parameters of each simulation: the minimum of the Toomre Q, the minimum of the swing amplification parameter X, the disc-to-bulge ratio D/B and the halo-to-bulge ratio H/B, within $R_{\rm eff}$ (obtained by calculating the projected radius containing half the mass of the bulge), and the Sérsic index n of the bulge. In the right part of the table, we show the parameters of the evolved system: the bar amplitude $A_{\rm bar}$ at t_1 and t_2, $R_{\rm eff}$ at $t_0 = 0$, t_1 and t_2, the fractional change in mass $\Delta M(B+D)/M(B+D)_{\rm init}$ within $R_{\rm eff}$ at t_1 and t_2, the aperture velocity dispersion σ_e of bulge+disc particles measured within a circular aperture at t_0, t_1 and t_2 and the dispersion scatter $\Delta\sigma_{\rm e}$ of bulge+disc particles at t_2. Simulations 16 and 21 are very similar in their setup; coincidentally, the effects of stochastically (Sellwood & Debattista 2009; Roškar et al. 2012) are weak in these two baryon-dominated simulations. t_0, t_1 and t_2 are $t = 0$, 2.5 and 5 Gyr, respectively.

Run	Q	X	D/B	H/B	n	$A_{\rm bar}$	$A_{\rm bar}$	$R_{\rm eff}(t_0)$	$R_{\rm eff}(t_1)$	$R_{\rm eff}(t_2)$	$\frac{\Delta M(B+D)}{M(B+D)_{\rm init}}$	$\frac{\Delta M(B+D)}{M(B+D)_{\rm init}}$	$\sigma_{\rm e}(t_0)$	$\sigma_{\rm e}(t_1)$	$\sigma_{\rm e}(t_2)$	$\Delta\sigma_{\rm e}(t_2)$
						(t_1)	(t_2)	(pc)	(pc)	(pc)	(t_1)	(t_2)	(km s^{-1})	(km s^{-1})	(km s^{-1})	(km s^{-1})
1	1.02	2.58	5.8	0.02	1.0	0.140	0.134	593	489	494	0.31	0.34	102.0	142.0	144.4	7.1
2	1.01	2.98	4.8	0.05	1.3	0.176	0.180	659	570	572	0.24	0.29	102.5	137.4	142.0	9.4
3	1.00	3.41	4.5	0.04	1.7	0.117	0.167	649	599	599	0.21	0.28	108.9	136.7	144.8	9.6
4	1.04	3.71	3.8	0.06	1.5	0.177	0.247	751	682	665	0.19	0.27	103.7	129.6	140.8	10.9
5	1.13	4.41	3.6	0.11	1.7	0.116	0.219	780	748	727	0.12	0.21	105.9	120.1	133.0	9.5
6	1.27	2.61	5.9	0.02	1.2	0.222	0.270	649	561	552	0.25	0.34	103.7	135.8	145.3	12.5
7	1.25	2.99	5.0	0.03	1.6	0.138	0.212	610	542	541	0.23	0.30	105.3	133.5	140.9	9.6
8	1.25	3.51	4.8	0.15	1.3	0.149	0.220	596	537	536	0.18	0.26	107.4	129.8	140.9	10.3
9	1.24	3.95	3.6	0.08	1.7	0.111	0.178	738	726	704	0.10	0.21	107.2	116.2	131.1	7.8
10	1.26	4.46	3.7	0.18	1.8	0.006	0.139	752	774	748	0.02	0.12	108.9	108.0	120.9	7.1
11	1.41	2.51	6.3	0.02	1.4	0.121	0.137	456	440	440	0.17	0.25	115.2	132.8	142.7	6.9
12	1.50	3.03	4.8	0.03	1.3	0.164	0.134	531	495	498	0.14	0.18	109.4	128.2	131.9	6.2
13	1.50	3.51	6.4	0.20	1.0	0.260	0.265	727	656	633	0.21	0.29	94.6	117.4	126.4	11.0
14	1.50	4.00	5.5	0.26	1.0	0.176	0.267	841	732	721	0.25	0.31	95.9	120.4	129.0	11.4
15	1.49	4.49	5.4	0.33	1.1	0.246	0.308	841	783	745	0.16	0.27	97.6	115.7	130.2	12.6
16	1.55	2.77	5.6	0.02	1.4	0.138	0.137	600	551	549	0.18	0.22	106.3	124.6	128.9	7.5
17	1.70	3.06	5.0	0.03	1.3	0.175	0.213	646	591	582	0.16	0.22	104.4	122.3	129.4	9.4
18	1.76	3.49	5.3	0.13	1.2	0.233	0.303	744	685	658	0.18	0.29	100.2	119.1	131.5	12.1
19	1.75	4.00	3.6	0.09	1.6	0.060	0.165	700	715	695	0.05	0.15	109.0	111.4	125.1	7.7
20	1.76	4.50	4.2	0.14	1.2	0.109	0.290	690	685	656	0.06	0.19	104.9	111.0	129.9	13.2
21	1.55	2.77	5.6	0.02	1.4	0.138	0.137	600	551	549	0.18	0.22	106.3	124.6	128.9	7.5
22	1.76	3.18	5.1	0.05	1.4	0.184	0.274	686	623	613	0.19	0.28	103.9	123.1	133.2	11.3
23	1.95	3.59	4.6	0.06	1.5	0.138	0.239	644	620	599	0.11	0.21	105.3	116.2	128.9	10.4
24	2.01	4.01	3.6	0.07	1.5	0.135	0.224	645	627	607	0.10	0.17	108.2	117.4	129.2	9.5
25	1.99	4.52	3.8	0.15	1.4	0.006	0.051	589	615	635	0.03	0.05	111.2	110.8	112.5	3.0

where κ is the epicyclic radial frequency, G is the gravitational constant, Σ is the surface density, R is the radius and m is the azimuthal mode number of the perturbation (Toomre 1981, 1964; Goldreich & Tremaine 1978, 1979). Here, we take $m = 2$ since we are interested in bars. We select 25 models that span the region of the $Q-X$ plane where the PDF is non-negligible ($1.0 \lesssim Q \lesssim 2.0$ and $2.5 \lesssim X \lesssim 4.0$) (see section 7 of W08). The properties of the models are summarized in Table 2 while the symbols used to represent each model are shown in Fig. 1. For instance, a plus ('+') symbol is used to represent model 1 throughout the paper.

The models do not contain an SMBH since an initial SMBH satisfying the $M_\bullet - \sigma_e$ relation would have a mass of only $\sim 10^7\,{\rm M}_\odot$. The influence radius of this SMBH would be $GM_\bullet/\sigma^2 \approx 10\,{\rm pc}$, which is smaller than the softening length used. We assume in our analysis that the SMBH initially satisfies the $M_\bullet - \sigma_e$ relation but retains this mass as the bar evolution proceeds. With this assumption we can compute the effect of bar evolution on the $M_\bullet - \sigma_e$ relation; comparing with observations then allows us to assess whether there is evidence of SMBH growth along with the bar.

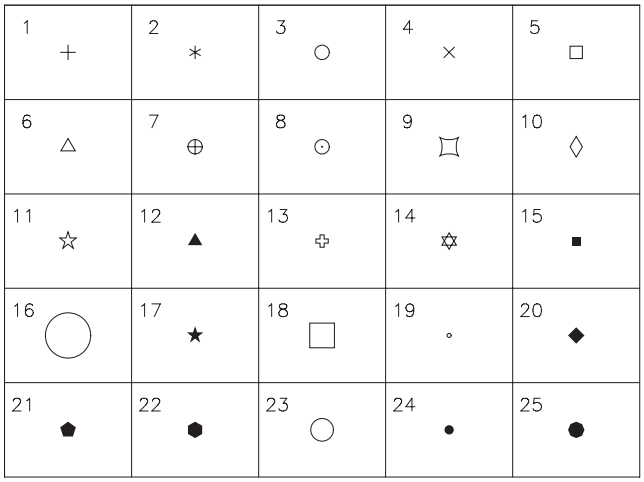

Figure 1. A grid of identifying symbols used to represent each model in the various plots of this paper.

2.3 Numerical parameters

The bulge, disc and halo consist of 2×10^5, 6×10^5 and 1×10^6 particles, respectively. Each population has equal mass particles, varying between simulations in the ranges 1.9-6.4 $\times\, 10^5 {\rm M}_\odot$ for the dark particles, 0.3-0.6 $\times\, 10^5 {\rm M}_\odot$ for the bulge particles and 0.4–0.7 $\times\, 10^5 {\rm M}_\odot$ for the disc particles. The range in mass resolution reflects the range in disc, halo and bulge masses across the 25 models considered here, see Table 2 and W08. The particle softening $\epsilon = 25\,{\rm pc}$ for all particles and the models were evolved for 10^4 equal time steps of length $\Delta t = 0.5$ Myr. The 25 models were

evolved for 5 Gyr using the parallel *N*-body tree code described in Dubinski (1996).

3 EVOLUTION OF CENTRAL DENSITY AND VELOCITY DISPERSION

All the models formed bars. We measure the bar amplitude, $A_{\rm bar}$, as the normalized amplitude of the $m = 2$ Fourier moment of the surface density of disc particles:

$$A_{\rm bar} = N_{\rm d}^{-1} \left| \sum_{j \in {\rm disc}} {\rm e}^{2{\rm i}\phi_j} \right|, \quad (9)$$

where ϕ_j is the two-dimensional cylindrical polar angle in the equatorial plane of the disc for the jth particle, and $N_{\rm d}$ is the total number of disc particles. We consider three different times in the simulations $t_0 = 0$, $t_1 = 2.5$ Gyr and $t_2 = 5$ Gyr and refer to these times throughout the paper. In most simulations, the bar forms by 1 Gyr and continues to grow until t_2 (see fig. 17 in W08), while in simulations 1 and 12 the bar amplitude peaks at 0.5 and 2 Gyr, respectively, and declines slightly thereafter. Simulation 10 does not form a bar by t_1 but a bar grows by t_2. The bar in simulation 25 also forms after t_1 but it is still very weak at t_2; thus, this simulation provides a control showing that in the absence of a strong bar, velocity dispersions, mass distributions, etc., do not evolve significantly. We have also confirmed that the velocity dispersions did not evolve significantly in an additional simulation generated with the same initial conditions code and which remained unbarred for 5 Gyr. Values of $A_{\rm bar}$ at t_1 and t_2 are given in Table 2.

We obtain the bulge $R_{\rm eff}$ by calculating the face-on projected circular aperture containing half of the bulge particles. We also measured $R_{\rm eff}$ by fitting a Sérsic profile to the mass-weighted surface density profile and found consistent values. We find $R_{\rm eff}$ in the range $456\,{\rm pc} < R_{\rm eff} < 841\,{\rm pc}$ at t_0, decreasing to $439\,{\rm pc} < R_{\rm eff} < 747\,{\rm pc}$ at t_2, except in simulation 25, where $R_{\rm eff}$ increases slightly (see Table 2). Throughout the paper all measurements, including those for the disc (D) and bulge+disc ($B + D$), are computed within $R_{\rm eff}$ *of the bulge* (B).

The formation and growth of a bar leads to the outward transport of angular momentum (Debattista & Sellwood 2000; Athanassoula 2002) resulting in an increase in the mass fraction of the disc in the central region, as was originally shown by Hohl (1971). We quantify the fractional change in the mass of the central region by defining $\Delta M/M_{\rm init} = (M_t - M_{\rm init})/M_{\rm init}$, where M_t is the mass within $R_{\rm eff}$ at either t_1 or t_2, and $M_{\rm init}$ is the mass within $R_{\rm eff}$ at t_0. The contribution of the halo mass within $r < R_{\rm eff}$ is less than 25 per cent of the total mass; we therefore neglect the dark matter particles in our analysis. We measure the change in angular momentum by defining $\Delta J_z(D)/J_{z,{\rm init}}(D) = (J_{z,t}(D) - J_{z,{\rm init}}(D))/J_{z,{\rm init}}(D)$, where $J_{z,t}(D)$ is the angular momentum at t_1 or t_2 of disc particles within $R_{\rm eff}$ and $J_{z,{\rm init}}(D)$ is the angular momentum at t_0 of all disc particles within $R_{\rm eff}$. We use $R_{\rm eff}$ for bulge particles measured at t_2 in order that the changes plotted are due to a difference in angular momentum, rather than different radial range. In Fig. 2, we show that the fractional change of the total angular momentum leads to an increase in the central mass of the disc and that the change in angular momentum reaches ~ -90 per cent by t_2. The evolution driven by the bar results in a transfer of angular momentum from small radii to large radii, and a growth in the central disc mass.

In the top row of Fig. 3, we plot the fractional change in mass, $\Delta M/M_{\rm init}$, versus the bar strength $A_{\rm bar}$. The increase in mass of the disc particles (Fig. 3, top left) shows a large scatter, with many

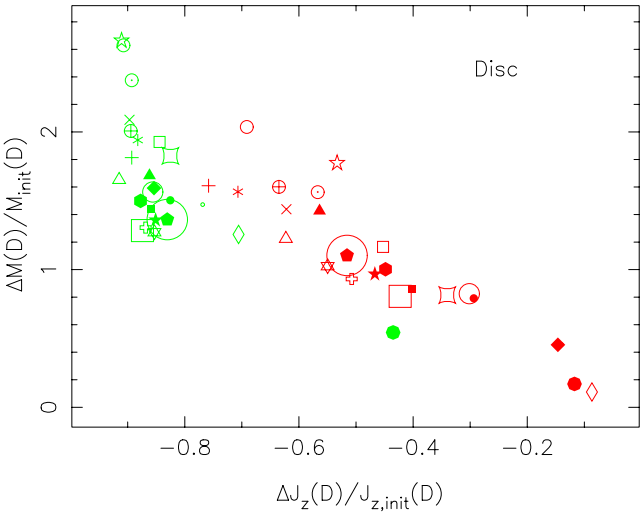

Figure 2. The fractional change in mass of the disc within the bulge $R_{\rm eff}$ (at t_2) plotted versus the changes in total angular momentum at t_1 in red and at t_2 in green.

models increasing by a factor of 1.5–2 by t_2. The top-right panel shows that the fractional mass increase for disc+bulge particles instead correlates with bar strength. The bulge-to-disc mass ratio within $R_{\rm eff}$ is $2.8 \lesssim B/D(R < R_{\rm eff}) \lesssim 8.8$ initially, decreasing to $1.2 \lesssim B/D(R < R_{\rm eff}) \lesssim 7.7$ by t_2. Fig. 3 shows that for model 25, the disc density and velocity dispersion at t_1 (prior to bar formation) are essential the same as they were initially. By t_2, a weak bar has formed and the disc concentration and velocity dispersion both rise slightly.

3.1 Measuring velocity dispersions

The increase in the central density deepens the potential and raises the velocity dispersion σ_e (Debattista et al. 2013). We define σ_e as the mass-weighted aperture velocity dispersion within a circular aperture of radius $R_{\rm eff}$:

$$\sigma_e{}^2 = \frac{\int_0^{R_{\rm eff}} I\,(R)\left(\sigma_{\rm los}^2\,(R) + \bar{v}_{\rm los}^2\,(R)\right){\rm d}R}{\int_0^{R_{\rm eff}} I(R){\rm d}R}, \quad (10)$$

where $I(R)$ is the mass density, $\sigma_{\rm los}$ is the standard deviation and $\bar{v}_{\rm los}$ is the mean line-of-sight velocity of particles within $R_{\rm eff}$. For a particle distribution, this becomes

$$\sigma_e{}^2 = \frac{\sum_{r_i \le R_{\rm eff}} m_i\, v_{i,{\rm los}}^2}{\sum_{r_i \le R_{\rm eff}} m_i}, \quad (11)$$

where r_i is the radius, m_i is the mass and $v_{i,los}$ is the line-of-sight velocity of the ith particle and the sum is over all particles within the circular aperture.

For each model, we measure σ_e for four different bar position angles PA = 0° (bar seen side-on), 30°, 60° and 90° at four inclinations $i = 0°$ (face-on), 30°, 60°, 90° (edge-on). We define $\langle\sigma_{\rm e}\rangle$ as the average of σ_e measured over the various orientations. The standard deviation of σ_e over all viewing angles is defined as the scatter $\Delta\sigma_{\rm e}$. In Fig. 3 (bottom row), we plot the average ratio of final to initial velocity dispersion, $\langle\sigma_{\rm e}/\sigma_{e0}\rangle$, versus $A_{\rm bar}$, where σ_{e0} is σ_e at t_0. Generally, σ_e increases with increasing bar strength, with $\sigma_e(B + D)$ increasing by as much as ~40 per cent. The models evolve along the (relatively weak) correlation. We have verified that in the absence of bar formation the central density does not evolve

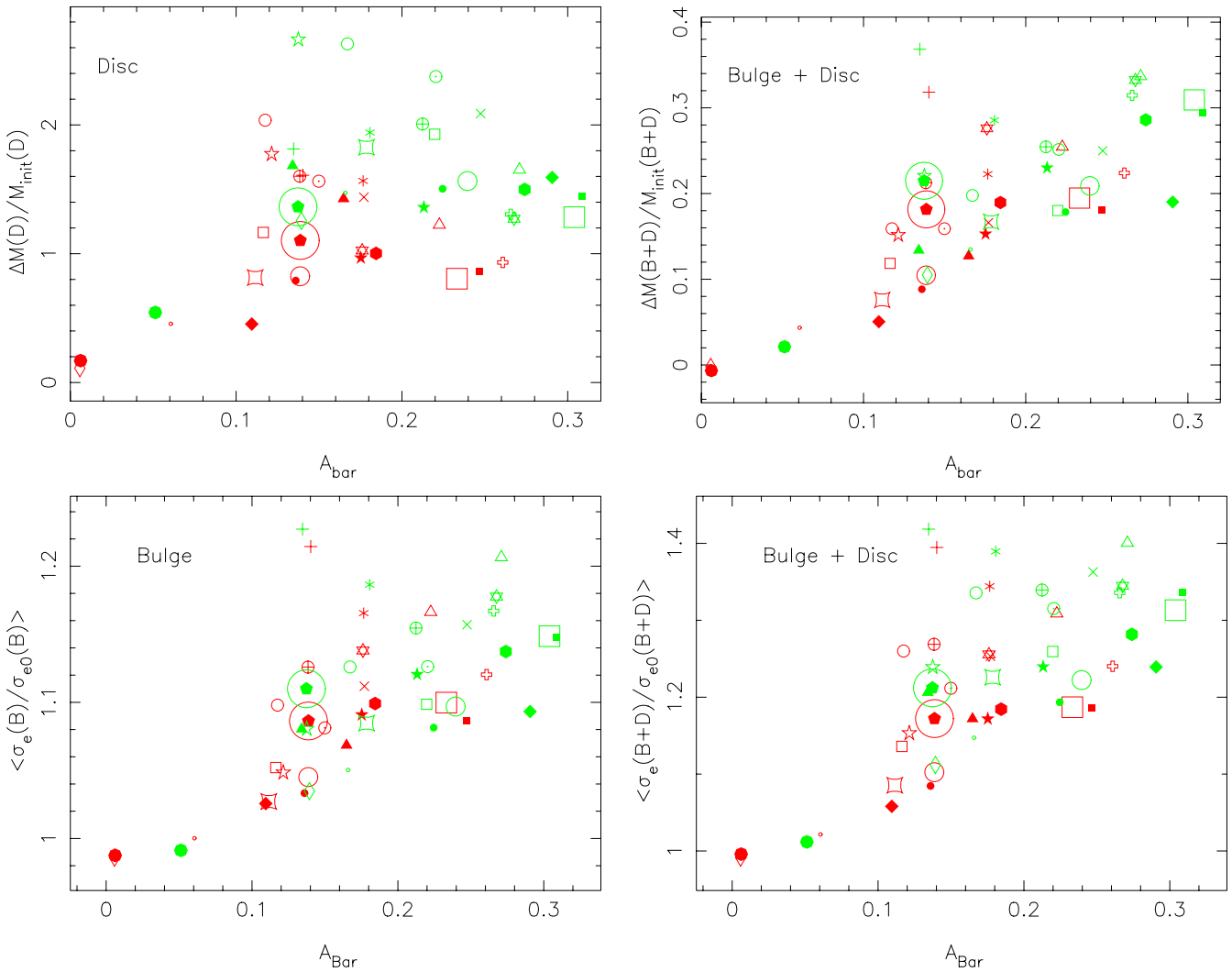

Figure 3. Top row: the fractional changes in the mass of the disc (left-hand panel) and bulge+disc (right-hand panel) within $R_{\rm eff}$ of the bulge plotted versus the bar amplitude $A_{\rm bar}$. Bottom row: the average ratio of final to initial velocity dispersion, $\langle\sigma_{\rm e}/\sigma_{\rm e0}\rangle$, for bulge particles (left-hand panel) and for bulge+disc particles (right-hand panel) versus $A_{\rm bar}$. In all panels, values at t_1 are shown in red, and at t_2 in green.

substantially and σ_e barely changes. We note also that bar formation was delayed till after t_1 in run 25 and the bar that forms is quite weak (see W08). Fig. 3 shows that σ_e and the mass distribution barely change after 2.5 Gyr for this model without a bar confirming that the initial conditions are in equilibrium.

3.2 The effect of disc contamination on velocity dispersions

Assuming that the fundamental parameter which determines $M_\bullet$ is σ_e of the bulge only, disc contamination of σ_e measurements can lead to offsets in the $M_\bullet - \sigma_e$ relation for any galaxy. Naively, one way of reducing this contamination might seem to be to use a smaller aperture since the ratio of bulge-to-disc mass within a given aperture generally increases as the aperture is made smaller. For instance, within $R_{\rm eff}/8$, the initial B/D of the models is $3.3 \lesssim B/D(R < R_{\rm eff}/8) \lesssim 47.9$ becoming $1.4 \lesssim B/D(R < R_{\rm eff}/8) \lesssim 13.4$ at t_2, which can be compared with the smaller values discussed above. We therefore test whether the effect of disc contamination to the dispersion can be reduced by using $\sigma_{e/8}$.

In Fig. 4, we compare $\sigma_e(B)$ with $\sigma_e(B+D)$ within $R_{\rm eff}$ (left-hand column) and $\sigma_{e/8}(B)$ with $\sigma_{e/8}(B+D)$ within $R_{\rm eff}/8$ (right-hand column) for four different inclinations. In all cases, the general effect of disc contamination is to increase the dispersion. This is, on average, a 10 per cent effect in face-on galaxies becoming ∼25 per cent for edge-on systems, in good agreement with Debattista et al. (2013). This is true for both σ_e and for $\sigma_{e/8}$. Surprisingly, the effect of disc contamination on $\sigma_{e/8}$ is about the same as on σ_e. In Fig. 5, we plot the cumulative distribution of $\sigma_{\rm e/8}(B+D)/\sigma_{\rm e/8}(B)$ and of $\sigma_{\rm e}(B+D)/\sigma_{\rm e}(B)$. The two distributions are very similar and the median of both distributions is ∼1.13. A Kolmogorov–Smirnov (K–S) test shows that the probability that the two distributions are identical is 0.88 showing that the aperture within which the velocity dispersion is measured has little effect on reducing the contamination from the disc. We also plot the distributions of $\Delta\sigma_{\rm e/8}(B+D)/\sigma_{\rm e/8}(B)$ and of $\Delta\sigma_{\rm e}(B+D)/\sigma_{\rm e}(B)$, which show that the scatter in $\sigma_{e/8}(B+D)$ is slightly larger than in $\sigma_e(B+D)$: the median of $\Delta\sigma_{\rm e/8}(B+D)/\sigma_{\rm e/8}(B)$ is 0.084 while for $\Delta\sigma_{\rm e}(B+D)/\sigma_{\rm e}(B)$ it is 0.077. The K–S test now finds that the probability that both distributions are identical is only 0.41.

We conclude that $\sigma_{e/8}$ does not provide any notable reduction in the amount of contamination by the disc, while increasing slightly the scatter in the measured dispersion. Moreover, smaller apertures

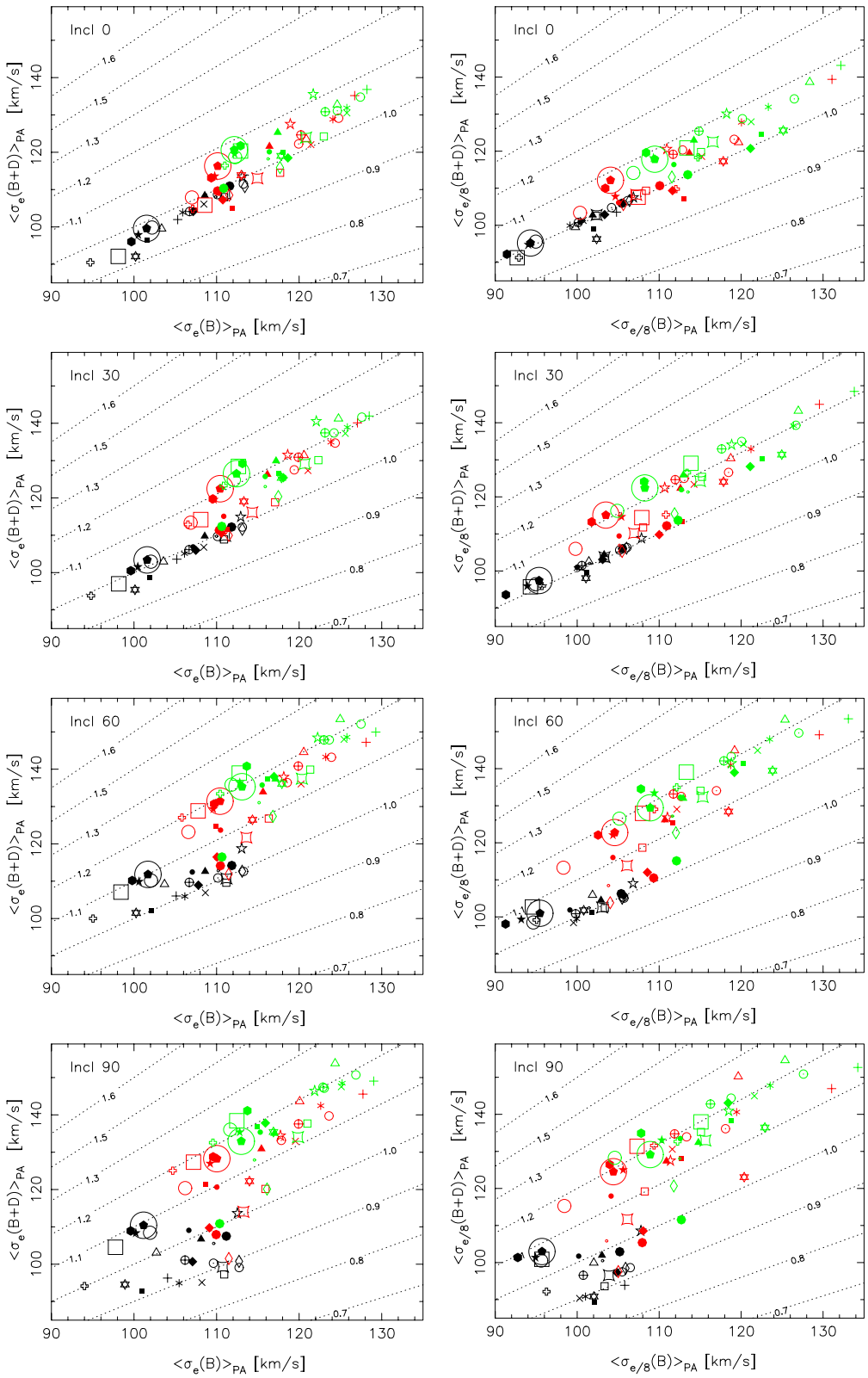

Figure 4. Mean $\sigma_e(B+D)$ versus mean $\sigma_e(B)$ (left-hand panels) and mean $\sigma_{e/8}(B+D)$ versus mean $\sigma_{e/8}(B)$ (right-hand panels). Black, red and green points represent the models at t_0, t_1 and t_2, respectively. We average over PA=0°, 30°, 60° and 90° and plot σ for inclinations $i = 0°$, 30°, 60° and 90° from top to bottom. Dotted lines have constant slope, as indicated along each line.

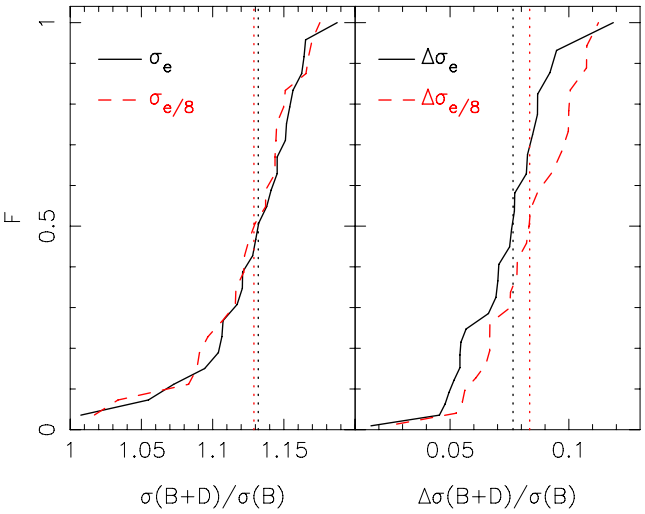

Figure 5. Left-hand panel: the cumulative distribution of $\sigma_{e/8}(B+D)/\sigma_{e/8}(B)$ (red dashed line) and $\sigma_e(B+D)/\sigma_e(B)$ (black solid line). Right-hand panel: the cumulative distribution of $\Delta\sigma_{e/8}(B+D)/\sigma_{e/8}(B)$ and $\Delta\sigma_e(B+D)/\sigma_e(B)$. The dotted lines show the median of each cumulative distribution. All distributions are shown at t_2.

are more likely to be contaminated by other nuclear components (e.g. Graham et al. 2011; McConnell & Ma 2013).

3.3 The effect of angular momentum redistribution on velocity dispersions

In Fig. 6, we plot $\langle\sigma_e/\sigma_{e0}\rangle$ versus $\Delta M(B+D)/M(B+D)_{\rm init}$, which now shows a strong correlation. For the correlation using $\sigma_e(B+D)$, we find a positive Spearman's rank correlation coefficient $r_s = 0.91$ which is statistically significant at more than 6σ while using $\sigma_e(B)$ we find an even stronger correlation with $r_s = 0.95$ corresponding to more than 7σ. This result is consistent with the findings of Debattista et al. (2013) who showed that an increase in disc mass within the bulge effective radius raises its velocity dispersion. The dotted lines in Fig. 6 indicate different values of $(\sigma_e/\sigma_{e0})^\beta$, where $\beta = 4.24$ comes from the $M_\bullet - \sigma_e$ relation of Gültekin et al. (2009). These lines indicate the factor by which SMBHs must grow in order to remain on the $M_\bullet - \sigma_e$ relation. The factors get to be as large as 2–3. A steeper $M_\bullet - \sigma_e$ relation (such as those of Graham et al. 2011 and McConnell & Ma 2013) would require even larger growth factors.

The presence of a bar inherently leads to an anisotropic velocity ellipsoid, which however cannot become too anisotropic before provoking bending instabilities, which drive the velocity ellipsoid closer to isotropy. We measure the velocity dispersions in cylindrical coordinates $\sigma_u, \sigma_v, \sigma_w$ and obtain the anisotropies $\beta_\phi = 1 - \sigma_v^2/\sigma_u^2$ and $\beta_z = 1 - \sigma_w^2/\sigma_u^2$. A positive value of β_ϕ or β_z implies that the radial velocity dispersion is larger than the tangential or vertical one. The initial bulge in all the models is isotropic by construction (classical bulges being well described by flattened isotropic rotators; Kormendy & Illingworth 1982; Davies & Illingworth 1983). Fig. 7 shows that following the formation of the bar, the velocity distributions of both the bulge and the disc particles become anisotropic, with the degree of anisotropy depending very weakly on the bar strength. When only the bulge is considered (left-hand panel) all runs show only a slight tangential anisotropy at t_2. There is a small amount of angular momentum transfer from the disc to the bulge, which explains why the bulge dispersion is skewed to slightly tangential velocities.

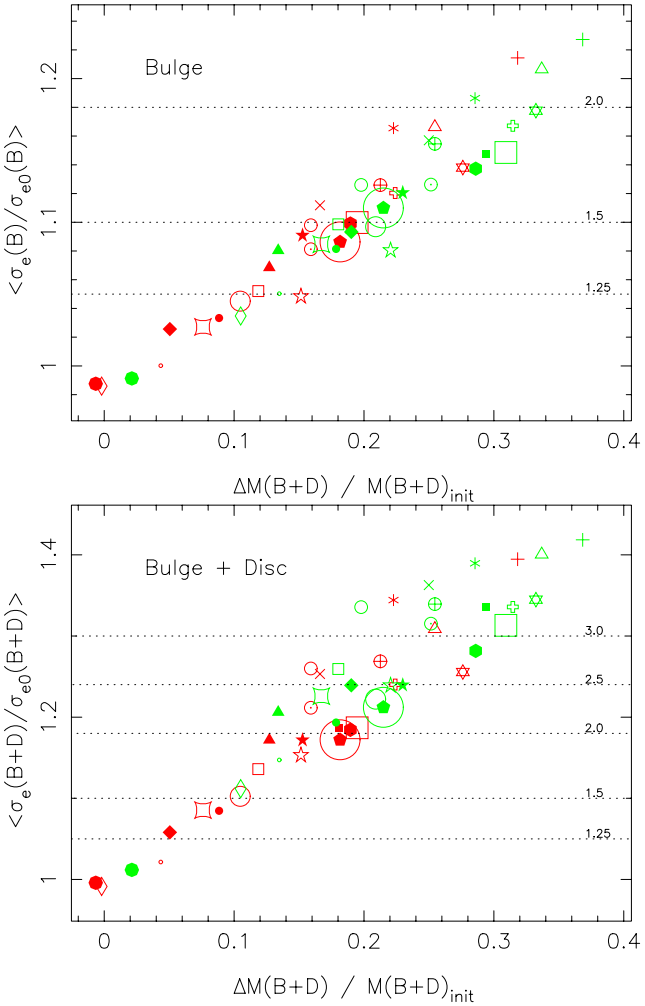

Figure 6. Average ratio of final to initial velocity dispersion at t_1 (red) and t_2 (green) for the bulge (top) and for the bulge+disc (bottom) versus the fractional change in mass of the bulge+disc within $R_{\rm eff}$. In both panels, the dotted lines indicate contours of constant $(\sigma_e/\sigma_{e0})^\beta$ for $\beta = 4.24$, with the values given above each line.

However, when both the bulge and disc are considered together, we measure a radial anisotropy up to $\beta_\phi(B+D) \sim 0.1$ and $\beta_z(B+D)$ reaching to $\sim$0.35. Bars being disc phenomena, it is disc stars which must support the bar, not bulge ones. Thus, the growth of a bar entails disc orbits becoming. Fig. 7 also shows that $\beta_\phi(B+D)$ is uncorrelated with $A_{\rm bar}$, while $\beta_z(B+D)$ shows a very weak correlation with $A_{\rm bar}$. The lack of dependence of β_ϕ and β_z on bar strength is probably a result of the buckling instability. As the degree of radial anisotropy increases the bar becomes unstable to the buckling instability, which results in a redistribution of kinetic energy and a decrease in anisotropy (Araki 1987; Raha et al. 1991; Merritt & Sellwood 1994).

Fig. 8 plots the orientation-averaged $\langle\sigma_e/\sigma_{e0}\rangle$ versus β_ϕ (top panels) and β_z (bottom panels). No correlation is present for bulge particles only (left-hand panels). However, a very strong correlation is present for bulge+disc particles and is stronger for $\beta_\phi(B+D)$ than for $\beta_z(B+D)$. The increase in σ_e is largest when $\beta_\phi(B+D)$ is largest, implying that the orbits contributing to the increased velocity dispersion are more radially biased. Since the correlation is absent when only bulge particles are considered the disc particles must be primarily responsible for the increased anisotropy (e.g. Saha,

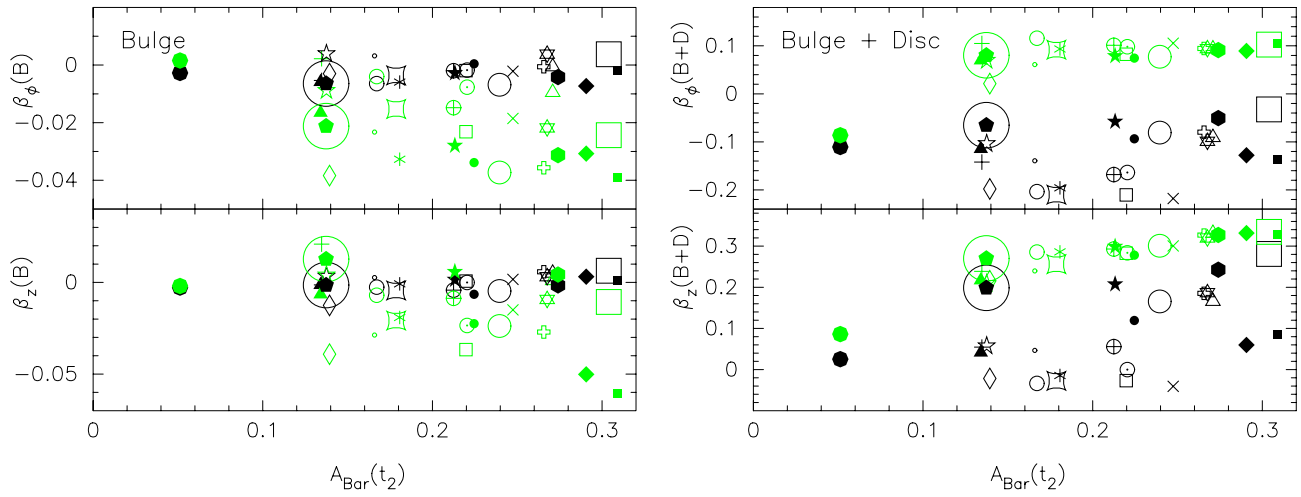

Figure 7. The anisotropies β_ϕ (top panels) and β_z (bottom panels) at t_0 (black) and t_2 (green) for bulge particles only (left-hand panels) and for the bulge+disc particles (right-hand panels) versus $A_{\rm bar}(t_2)$. Note that the initial disc has no bar, so $A_{\rm bar}$ is zero; in order to show the evolution of the anisotropy, we plot the initial anisotropies versus $A_{\rm bar}(t_2)$.

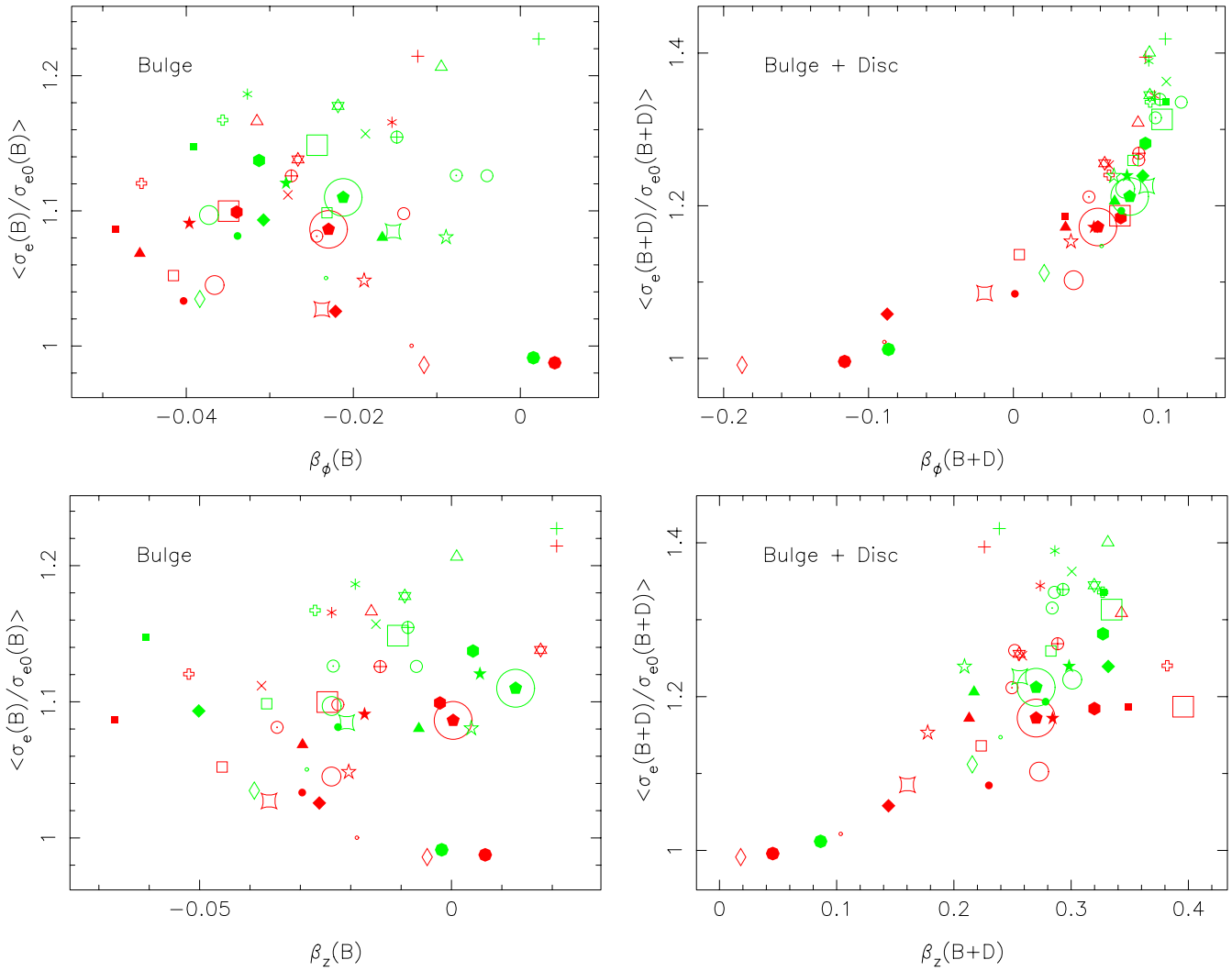

Figure 8. The ratio of final to initial velocity dispersion, $\langle\sigma_e/\sigma_{e0}\rangle$, versus anisotropy β_ϕ (top panels) and β_z (bottom panels) for the bulge particles only (left-hand panels) and for the bulge+disc particles (right-hand panels). In all panels, values at t_1 are red and at t_2 are green.

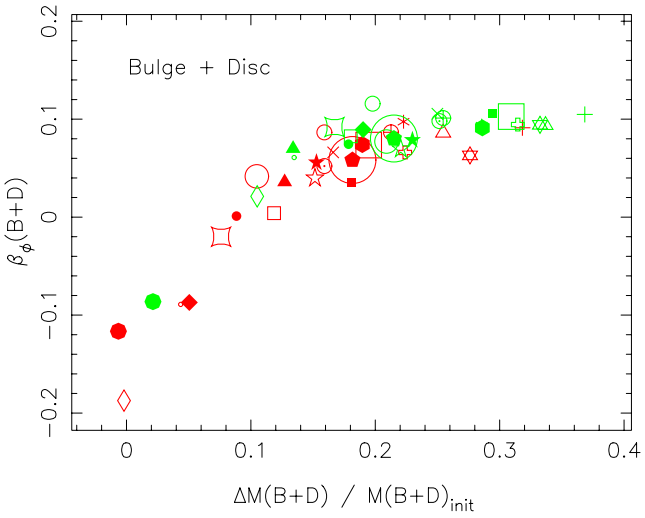

Figure 9. $\beta_\phi(B+D)$ versus the fractional changes in mass of the bulge+disc at t_1 (red) and t_2 (green).

Martinez-Valpuesta & Gerhard 2012). Fig. 8 also shows a temporal evolution, with the central regions becoming more anisotropic and σ_e increasing with time. Model 25 again stands out as barely evolving during this period, with the bulge remaining nearly isotropic.

In Fig. 9, we plot $\beta_\phi(B+D)$ versus the fractional change in mass which shows a strong correlation but with $\beta_\phi(B+D)$ saturating at ∼0.1 by t_2. The Spearman coefficient is $r_s = 0.67$; thus, this correlation is weaker than the correlation between $\langle\sigma_e/\sigma_{e0}\rangle$ and $\Delta M(B+D)/M(B+D)_{init}$, which is presumably more fundamental.

3.4 Effect of viewing orientation

Anisotropy increases the scatter in σ_e, $\Delta\sigma_e$ (Graham et al. 2011). In Fig. 10, we show the scatter in σ_e by averaging it over position angles at fixed inclinations, $\langle\Delta\sigma_e\rangle_{PA}$. We present results at t_1 which produces more fractional scatter than at t_2 in most cases (the exception being in model 10 in which the bar is still very weak at t_1). For bulge particles, $\Delta\sigma_e$ is ∼6 per cent but can be as large as ∼13 per cent for bulge+disc particles. The scatter increases with inclination and, at fixed inclination, with bar strength. In the face-on case, since we are measuring σ_e within circular apertures, $\Delta\sigma_e = 0$. A typical strong bar is therefore likely to have an ∼10 per cent effect on the scatter in σ_e, which will in turn lead to an increased scatter in the $M_\bullet$–σ_e relation.

4 PREDICTED EVOLUTION OF THE $M_\bullet$–σ_e RELATION

We have shown that the angular momentum redistribution of Fig. 2 is a driver of major change in σ_e. Changes in σ_e can lead to displacements of an SMBH in the $M_\bullet$–σ_e relation. In this section, we estimate the effects of this σ_e evolution on the $M_\bullet$–σ_e relation of barred galaxies. Since the models we use do not contain an SMBH we simply assume that $M_\bullet$ before the bar forms satisfies the $M_\bullet$–σ_e relation and explore what happens if $M_\bullet$ does not change after the bar forms. Moreover, in the absence of satellite accretion and star formation, our bulges do not grow in mass.

An increased σ_e moves a SMBH to the right of the $M_\bullet$–σ_e relation. If the average fractional change in σ_e is $\langle\sigma_e/\sigma_{e0}\rangle$, then we can write the $M_\bullet$–σ_e relation, assuming no $M_\bullet$ growth and that $\langle\sigma_e/\sigma_{e0}\rangle$

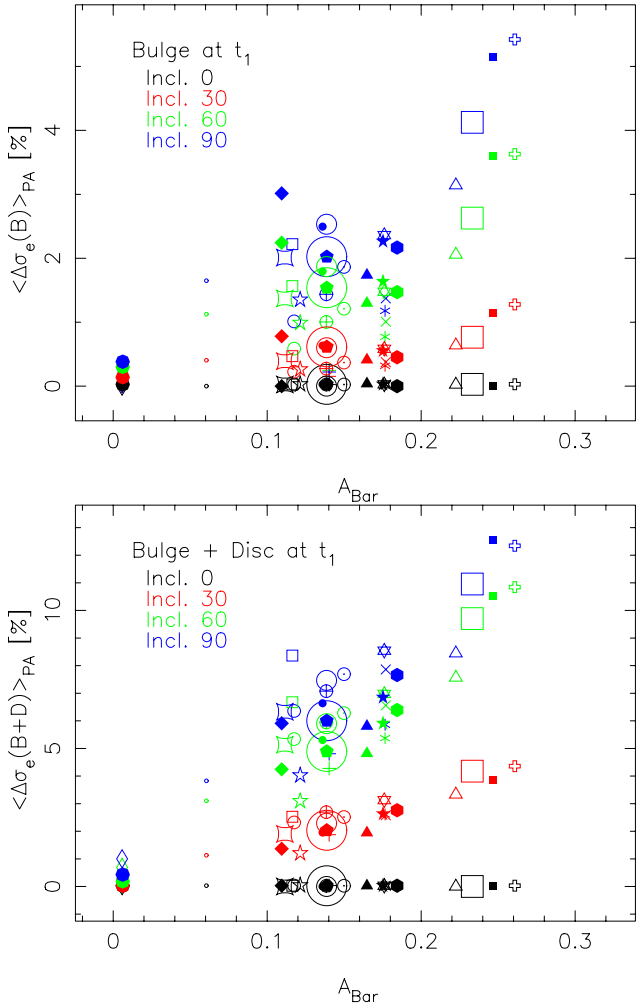

Figure 10. The scatter in the velocity dispersion averaged over PA at fixed inclination, $\langle\Delta\sigma_e\rangle_{PA}$, plotted versus bar amplitude at t_1. $\langle\Delta\sigma_e\rangle$ is measured within R_{eff} for bulge (top panel) and bulge+disc particles (bottom panel).

is independent of σ_{e0}, as $\log M_\bullet = \alpha + \beta\log\sigma_e - \beta\log\langle\sigma_e/\sigma_{e0}\rangle$. Thus, the slope of the $M_\bullet$–σ_e relation remains β, but the zero-point changes by

$$\delta\alpha = -\beta\log\langle\sigma_e/\sigma_{e0}\rangle \quad (12)$$

(see also Debattista et al. 2013). Since $\langle\sigma_e/\sigma_{e0}\rangle > 1$, the resulting $\delta\alpha < 0$, i.e. the new $M_\bullet$–σ_e relation will be offset below the $M_\bullet$–σ_e relation of unbarred galaxies. We measure $\langle\sigma_e/\sigma_{e0}\rangle = 1.12 \pm 0.05$ for bulge particles only ($\langle\sigma_e/\sigma_{e0}\rangle = 1.27 \pm 0.12$ for bulge+disc particles). This value of $\langle\sigma_e/\sigma_{e0}\rangle$ would result in offsets in the range $-\delta\alpha = 0.17$–0.27 (bulge particles only) or 0.36–0.57 (bulge+disc particles) for $\beta = 3.5$–5.5 if SMBHs do not grow further.

In Fig. 11, we plot the models in the $M_\bullet$–σ_e plane, adopting $\beta = 4.24$ from Gültekin et al. (2009), at t_0 (before the bars form) as black symbols and at t_2 (at the end of the simulation) as green points. We obtain $M_\bullet$ using $\sigma_e(B)$ at t_0. As expected, bar evolution without $M_\bullet$ growth shifts the models to the right. We measure the bar-induced offset by fitting the $M_\bullet$–σ_e relation using MPFITEXY,[1] which implements the algorithm MPFIT (Markwardt 2009), to obtain

[1] http://purl.org/mike/mpfitexy

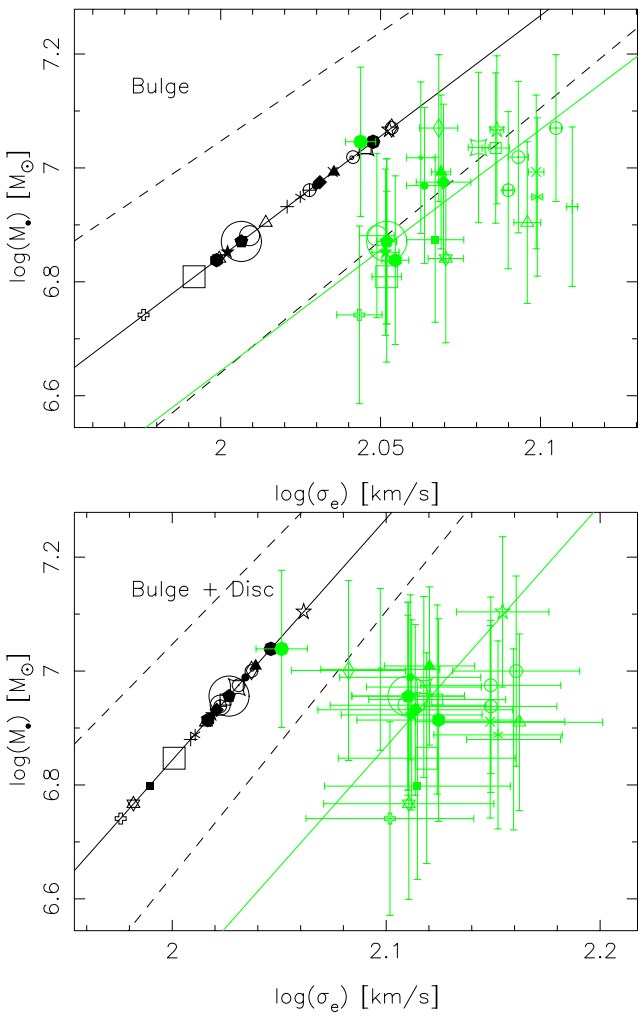

Figure 11. Using the $M_\bullet - \sigma_e$ relation of Gültekin et al. (2009, solid black line, with dashed lines indicating the one σ uncertainty), we show the initial σ_e and the corresponding $M_\bullet$ (black symbols) for the simulations. Then assuming that $M_\bullet$ does not change, we plot σ_e at t_2 (green symbols). The green solid line shows a fit to the green points using MPFITEXY with slope fixed to $\beta = 4.24$ to match the solid black line. The top panel uses $\sigma_e(B)$ while the bottom panel uses $\sigma_e(B+D)$. Note the different scale of the abscissa. In both cases, we find a substantial offset from the $M_\bullet - \sigma_e$ relation.

a linear regression by minimizing

$$\chi^2 = \sum_{i=1}^{N} \frac{(y_i - \alpha - \beta x_i)^2}{\epsilon_{x_i}^2 + \left(\epsilon_{y_i}^2 + {\epsilon_0}^2\right)}, \tag{13}$$

where ϵ_0 is the intrinsic scatter, which is determined such that the $\tilde{\chi}^2 \lesssim 1$ (Tremaine et al. 2002). We fit the $M_\bullet - \sigma_e$ relation for σ_e at t_2 assuming that $M_\bullet$ remains unchanged from t_0. For the errors on individual σ_e values we use $\Delta\sigma_e$. The errors in $M_\bullet$ are obtained from $\sigma_e \pm \Delta\sigma_e$ at t_0. We assume in these fits that the $M_\bullet - \sigma_e$ relation of barred galaxies has the same $\beta = 4.24$ as do the unbarred galaxies, and therefore hold β fixed. A significant offset develops regardless of whether we measure $\sigma_e(B)$ or $\sigma_e(B+D)$. We find an offset $\delta\alpha \simeq -0.20$ (see Table 3). Since the scatter in the observed $M_\bullet - \sigma_e$ relation is generally estimated at $\epsilon_0 = 0.3 - 0.45$ (see Table 1), an offset of this magnitude is likely to be hard to measure.

We find a scatter of $\epsilon_0 \simeq 0.1$ in the simulations due to the different relative increases in central mass in the different models. The full scatter predicted by the models includes that from viewing orientation, which from the top-right panel of Fig. 10 we estimate at 0.05–0.09. Thus, together with the scatter due to viewing orientation the predicted total increase in scatter relative to the intrinsic scatter in the $M_\bullet - \sigma_e$ relation of unbarred galaxies is 0.15–0.16, which must be added in quadrature to the intrinsic scatter to obtain the predicted scatter in the $M_\bullet - \sigma_e$ under our assumptions.

Table 3. Results of fitting the $M_\bullet - \sigma_e$ relation of the simulations assuming no $M_\bullet$ growth from a relation with $\beta = 4.24$ (Gültekin et al. 2009) at t_0. The offset is the difference between the zero-point of unbarred disc galaxies and from the fit to the barred models at t_2. The scatter is ϵ_0 of equation (13).

Component	α	Offset ($\delta\alpha$)	Scatter (ϵ_0)
Bulge	7.92 ± 0.03	-0.20	0.09
Bulge+Disc	7.91 ± 0.03	-0.21	0.11

4.1 Residuals correlations

The main parameter that governs how much σ_e increases, and thus how far a barred galaxy strays from the $M_\bullet - \sigma_e$ relation, is the fractional change of total mass within the bulge effective radius (Debattista et al. 2013, and Fig. 6 here). Unfortunately, this is not directly observable because we can never know what any galaxy looked like before the bar formed. We have searched for observationally accessible structural parameters that correlate with $\Delta M(B+D)/M(B+D)_{\rm init}$. It seems not unreasonable to expect that $M(B)/M(B+D)$ within $R_{\rm eff}$ (note, this is *not* the usual bulge-to-total ratio, B/T) correlates with $\Delta M(B+D)/M(B+D)_{\rm init}$. The top panel of Fig. 12 therefore plots the $M_\bullet - \sigma_e$ residuals, $\delta\log \mathrm{M}_\bullet$, as a function of $M(B)/M(B+D)$. A clear correlation is evident, with the Spearman coefficient $r_{\rm s} = 0.91$ at t_1 and $r_{\rm s} = 0.90$ at t_2. Jointly, $t_1 + t_2$ produce a correlation with $r_{\rm s} = 0.89$, which is statistically significant at more than 6σ.

Alternatively, we have already shown in Figs 8 and 9 that the anisotropies correlate with the change in σ_e and with the fractional mass change. Thus, rather than a structural parameter, a kinematic one may provide an alternative indication of the offset of a barred galaxy from the $M_\bullet - \sigma_e$ relation. Note however that Fig. 7 shows that the anisotropy of the bulge component only is not much changed by the bar, and Fig. 8 shows that $\beta_\phi(B)$ and $\beta_z(B)$ do not correlate with $\langle\sigma_{\rm e}/\sigma_{e0}\rangle$. It is therefore the anisotropy of the bulge+disc that must be measured to determine the offset. The bottom panel of Fig. 12 plots $\delta\log \mathrm{M}_\bullet$ as a function of $\beta_\phi(B+D)$; we find a Spearman coefficient $r_{\rm s} = -0.89$ at t_1 and $r_{\rm s} = -0.82$ at t_2, with a joint $(t_1 + t_2)$ $r_{\rm s} = -0.85$ corresponding to almost 6σ significance. The strength of the correlation between $\delta\log \mathrm{M}_\bullet$ and $\beta_z(B+D)$, instead, has $r_{\rm s} = -0.66$ at t_1 and $r_{\rm s} = -0.61$ at t_2, with a joint $r_{\rm s} = -0.64$ corresponding to more than 4σ significance.

A concern with the correlation between $M(B)/M(B+D)$ and $\Delta M(B+D)/M(B+D)_{\rm init}$ is that it could be weakened if models with a larger range of B/D at t_0 were included. Moreover, while we can easily compute $M(B)/M(B+D)$ in the simulations, the same quantities may be non-trivial in observations because once the bar forms the density profile of the disc need no longer be an exponential extending to small radii (e.g. Debattista et al. 2006). The main limitation of using $\beta_\phi(B+D)$ to measure the residuals instead is that it tends to saturate, at least in these collisionless simulations. In addition, in a companion paper, Brown et al. (2013) show that the

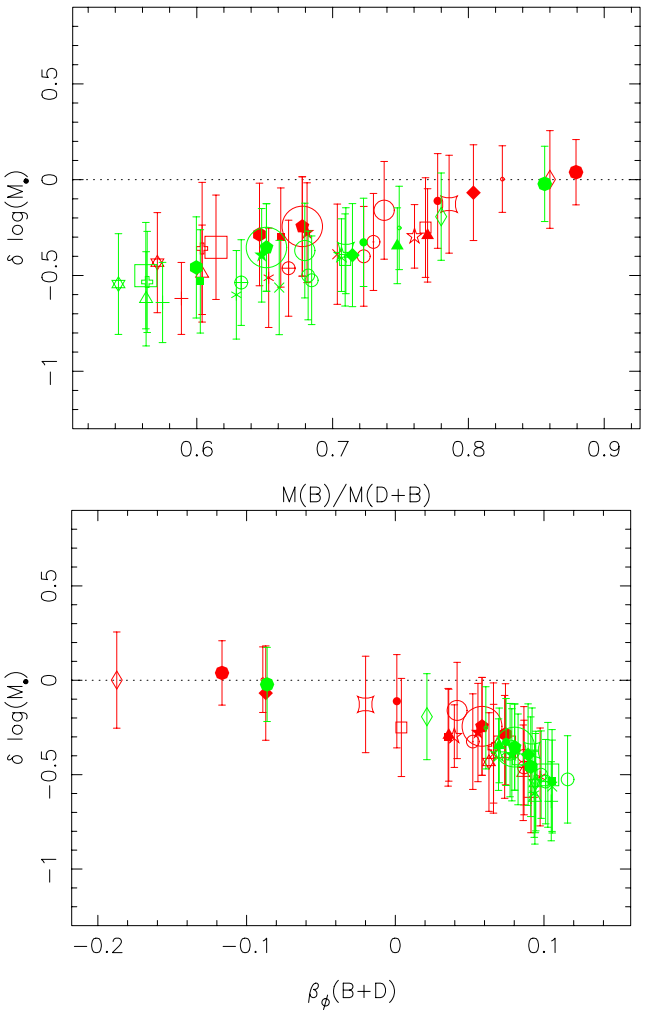

Figure 12. The residuals of the simulations from the $M_\bullet - \sigma_e$ relation. Values are indicated in red at t_1 and in green at t_2. Top: plotted as a function of $M(B)/M(B+D)$. Bottom: plotted as a function of $\beta_\phi(B+D)$.

growth of a central massive object inside a barred galaxy will tend to isotropize the velocity distribution. Star formation will also change the velocity distribution but it is still unknown how. Nonetheless, we propose that modelling the velocity anisotropy is worthwhile in order to understand the offsets of barred galaxies from the $M_\bullet - \sigma_e$ relation.

5 COMPARISON WITH OBSERVATIONS

Observational evidence for an offset in the $M_\bullet - \sigma_e$ relation of barred galaxies has been presented by a number of authors (Hu 2008; Graham 2008a; Graham et al. 2011). Guided by the results above, in this section we test for an offset in the observational data by fixing the slope of the barred $M_\bullet - \sigma_e$ relation to that of unbarred galaxies and measuring the zero-point.

5.1 Sample selection

We have assumed that SMBHs are present in bulges and satisfy the $M_\bullet - \sigma_e$ relation before the bar forms, and that the bulges do not grow any further once the bar forms. Both these assumptions imply that classical bulges are more suited to compare with the simulations. Classical bulges share structural and kinematical properties with elliptical galaxies (e.g. Wyse, Gilmore & Franx 1997; Kormendy & Kennicutt 2004; Gadotti 2009), with both types of spheroids appearing in similar positions on the Fundamental Plane defined by the central velocity dispersion, the central surface brightness and the effective radius (Bender, Burstein & Faber 1992). Pseudo-bulges instead are more closely related to the discs of their host galaxy (see Kormendy & Kennicutt 2004 for a review). While elliptical galaxies and classical bulges are believed to form via mergers of galaxies and accretion (Eggen & Sandage 1962; Tremaine, Ostriker & Spitzer 1975; Searle & Zinn 1978; Kauffmann, White & Guiderdoni 1993; Baugh, Cole & Frenk 1996; van den Bosch 1998; Naab et al. 2007), pseudo-bulges are thought to form via secular processes in the disc which are driven by non-axisymmetric structures such as bars and spirals (Combes & Sanders 1981; Combes et al. 1990; Raha et al. 1991; Courteau et al. 1996; Norman, Sellwood & Hasan 1996; Bureau & Athanassoula 1999; Debattista et al. 2004; Athanassoula 2005; Drory & Fisher 2007). The difference between classical- and pseudo-bulges is reflected also in their SMBH scaling relations. Hu (2008) and Debattista et al. (2013) found that SMBHs in elliptical galaxies and in classical bulges follow a similar $M_\bullet - \sigma_e$ relation. Pseudo-bulges instead either have a significant offset from this $M_\bullet - \sigma_e$ relation (Hu 2008; Graham 2008b) or no $M_\bullet - \sigma_e$ relation at all (Kormendy, Bender & Cornell 2011).

In this work, we therefore distinguish observed galaxies by whether they contain a classical- or a pseudo-bulge. We use data from the literature to compile samples of unbarred classical bulges and barred classical bulges with $M_\bullet$ measurements. Purely for the sake of comparison, we also compile a sample of barred pseudo-bulges. The final sample of galaxies is listed in Table 4. Our sample of $M_\bullet$ and σ_e measurements is primarily drawn from the compilation of McConnell & Ma (2013), with one galaxy (NGC 7457) from Gültekin et al. (2009) and another (NGC 3414) from Graham & Scott (2013). We correct the value of σ_e for NGC 1300 found in McConnell & Ma (2013), who list $\sigma_e = 218 \pm 10\,\mathrm{km\,s^{-1}}$; the correct value is $\sigma_e = 87 \pm 5\,\mathrm{km\,s^{-1}}$ (Batcheldor et al. 2005). We largely rely on the *morphological* classification of Fisher & Drory (2008, 2010, 2011). For some bulges, our classification is based solely on Sérsic index $n > 2$ of a bulge+disc decomposition. For these cases, we use unpublished fits provided to us by David Fisher supplemented by fits by Beletsky et al. (2011), Rusli et al. (2011), Fabricius et al. (2012) and Krajnović et al. (2013). We classify the Milky Way as having a pseudo-bulge although this is controversial; the bulge+disc decomposition is based on the model of Bissantz & Gerhard (2002). From the sample of disc galaxies in McConnell & Ma (2013), we exclude those where the bulge classification is unknown or where the galaxy is unbarred and hosts a pseudo-bulge. We exclude NGC 4826 from our sample because of confusion over its bulge type (Fabricius et al. 2012), and NGC 2549 because the only available profile fit uses only a single Sérsic (Krajnović et al. 2013). We exclude another 10 barred galaxies because no bulge+disc fits are available but include them in a separate unclassified bulge barred galaxy sample. Table 4 presents our samples of galaxies, consisting of 12 unbarred galaxies with classical bulges, 5 barred galaxies with classical bulges and 9 barred galaxies with pseudo-bulges.

5.2 The $M_\bullet - \sigma_e$ relation of unbarred classical bulges

Using MPFITEXY, we first fit the $M_\bullet - \sigma_e$ relation for the unbarred classical bulges. The full parameters of the fit are listed in Table 5; we obtain a slope $\beta = 3.78 \pm 0.31$. Remarkably, this sample of 12 galaxies chosen purely by their morphology have a quite small

Table 4. Published values for the black hole mass and bulge velocity dispersion for the galaxies plotted in Fig. 13.

Galaxy	Type	Bulge classification[a]	Sérsic index n	B/D	$M_\bullet$ (10^8 M$_\odot$)	σ_e (km s^{-1})
Unbarred						
NGC 1332[1,7,13]	S0	C	2.36	0.79	15 ± 2	328 ± 16
M81 (NGC 3031)[1,4b]	Sb	C	3.88 ± 0.23	0.59	$0.8^{+0.2}_{-0.11}$	143 ± 7
NGC 3115[1,4a]	S0	C	3.89 ± 0.32	1.63	$8.9^{+5.1}_{-2.7}$	230 ± 11
NGC 3245[1,4a]	S0	C	3.82 ± 0.34	1.44	$2.1^{+0.5}_{-0.6}$	205 ± 10
NGC 3414[2,6,10,13]	S0	C	2.3 ± 0.9	0.52	2.4 ± 0.3	236.8 ± 7.5
NGC 3585[1,4d, 13]	S0	C	3.49	2.23	$3.3^{+1.5}_{-0.6}$	213 ± 10
NGC 3998[1,4d, 8,13]	S0	C	4.1	1.38	8.5 ± 0.7	272 ± 14
NGC 4026[1,4d, 8,13]	S0	C	2.46	0.47	$1.8^{+0.6}_{-0.3}$	180 ± 9
NGC 4342[1,4d, 8,13]	S0	C	4.84	1.63	$4.6^{+2.6}_{-1.5}$	225 ± 11
NGC 4564[1,4a]	S0	C	3.70 ± 0.66	1.5	0.88 ± 0.24	162 ± 8
NGC 4594[1,4c]	Sa	C	6.2 ± 0.6	1.04	$6.7^{+0.5}_{-0.4}$	230 ± 12
NGC 7457[3,4b]	S0	C	2.72 ± 0.4	0.15	$0.041^{+0.012}_{-0.017}$	67 ± 3
Barred						
M31 (NGC 224)[1,4c, 12]	SBb	C	2.1 ± 0.5	0.92	$1.4^{+0.8}_{-0.3}$	160 ± 8
NGC 1023[1,4b]	SB0	C	2.47 ± 0.34	0.54	0.4 ± 0.04	205 ± 10
NGC 1316[1,5,13]	SB0	C	2.9	0.59	1.7 ± 0.3	226 ± 11
NGC 4258[1,4c, 11]	SABbc	C	2.80 ± 0.28	0.12	0.367 ± 0.001	115 ± 10
NGC 4596[1,4d, 13]	SB0	C	3.61	1.04	$0.84^{+0.36}_{-0.25}$	136 ± 6
MW[1]	SBbc	P	1.0	0.12	0.041 ± 0.006	103 ± 20
NGC 1068[2,15]	SBb	P	-	-	0.084 ± 0.003	151 ± 7
NGC 1300[1,4a]	SB(rs)bc	P	1.61 ± 0.39	0.09	$0.71^{+0.34}_{-0.18}$	87 ± 5
NGC 2787[1,4c, 15]	SB0	P	2.6 ± 0.5	1.38	$0.41^{+0.04}_{-0.05}$	189 ± 9
NGC 3227[1,4d, 15]	SBa	P	2.49	0.18	$0.15^{+0.05}_{-0.08}$	133 ± 12
NGC 3368[1,4b, 9]	SBab	P	1.63 ± 0.18	0.35	$0.076^{+0.016}_{-0.015}$	122^{+28}_{-24}
NGC 3384[1,4b]	SB0	P	1.42 ± 0.2	0.49	$0.11^{+0.05}_{-0.05}$	143 ± 7
NGC 3489[1,4b]	SAB0	P	1.47 ± 0.28	1.45	$0.06^{+0.008}_{-0.009}$	100^{+15}_{-11}
NGC 7582[1,4d, 13]	SBab	P	0.91	0.10	$0.55^{+0.16}_{-0.11}$	156 ± 19
Barred galaxies with no bulge classification						
IC2560[2,14]	SBb	–	–	–	$0.044^{+0.044}_{-0.022}$	144
NGC 253[2,10]	SBc	–	–	–	$0.10^{+0.10}_{-0.05}$	109 ± 20
NGC 2273[1]	SBa	–	–	–	0.078 ± 0.004	144^{+18}_{-15}
NGC 2549[1]	SB0	–	–	–	$0.14^{+0.01}_{-0.04}$	145 ± 7
NGC 2778[2,10]	SB0	–	–	–	$0.15^{+0.09}_{-0.1}$	161.7 ± 3.2
NGC 3393[1]	SBa	–	–	–	0.33 ± 0.02	148 ± 10
NGC 4151[2,15]	SBab	–	–	–	0.65 ± 0.07	119 ± 26
NGC 4945[2,10]	SBcd	–	–	–	$0.014^{+0.014}_{-0.007}$	127.9 ± 19.1
NGC 6323[1]	SBab	–	–	–	0.098 ± 0.001	158^{+28}_{-23}
UGC3789[1]	SBab	–	–	–	$0.108^{+0.006}_{-0.005}$	107^{+13}_{-12}

[a]C = classical, P = pseudo. Classifications take into account Sérsic index as well as bulge morphology except where indicated.
[1]Black hole masses and velocity dispersion data from McConnell & Ma (2013).
[2]Black hole masses and velocity dispersion data from Graham & Scott (2013).
[3]Black hole masses and velocity dispersion data from Gültekin et al. (2009).
[4a]Bulge/disc decompositions from Fisher & Drory (2008).
[4b]Bulge/disc decompositions from Fisher & Drory (2010).
[4c]Bulge/disc decompositions from Fisher & Drory (2011).
[4d]Bulge/disc decompositions from David Fisher (private communication).
[5]Bulge/disc decompositions from Beletsky et al. (2011).
[6]Bulge/disc decompositions from Krajnović et al. (2013).
[7]Bulge/disc decompositions from Rusli et al. (2011).
[8]Sérsic indices found by Krajnović et al. (2013) are <2. Those from Fisher & Drory (2010) are preferred because their data is based on *HST* observations which are of higher resolution than those of Krajnović et al. (2013) which are based on SDSS data and from imaging with the Wide Field Camera (WFC) mounted on the 2.5-m Isaac Newton Telescope. Bulge/disc decompositions based on lower resolution observations tend to give lower values of n therefore the value of n given for NGC 3414 may be trusted to classify its bulge as any error will tend to lower the value of n but it is still >2.
[9]Sérsic index found by Fabricius et al. (2012) is 2.46 ± 0.77 but morphologically classified as pseudo-bulge.
[10]Source data from HyperLeda (Paturel et al. 2003).
[11]Described as pseudo-bulge (possibly classical) in Fisher & Drory (2010) but we use the updated classification of Fisher & Drory (2011).
[12]For barred classification see Athanassoula & Beaton (2006).
[13]Classified only on basis of Sérsic index. $n > 2$ implies a classical bulge, $n < 2$ implies a pseudo-bulge.
[14]Velocity dispersion from Cid Fernandes et al. (2004); for fitting purposes we assume an uncertainty of ± 20 km s^{-1}.
[15]Bulge classification (and σ_e for NGC 1068) from Kormendy et al. (2011).

Table 5. Fit results: using the data of Table 4 to fit the $M_\bullet - \sigma_e$ relation of only classical bulges in unbarred galaxies. We then fix the resulting slope and fit only the zero-point to obtain the offset of classical bulges and pseudo-bulges in barred galaxies. *N* is the number of galaxies in each sample.

Sample	*N*	β	α	ϵ_0 (dex)
Unbarred classical bulges	12	3.78 ± 0.31	8.39 ± 0.05	0.11
Barred classical bulges	5	3.78	8.21 ± 0.19	0.41
Barred pseudo-bulges	9	3.78	7.91 ± 0.18	0.50
Barred classical bulges+ unclassifieds	15	3.78	7.89 ± 0.14	0.46

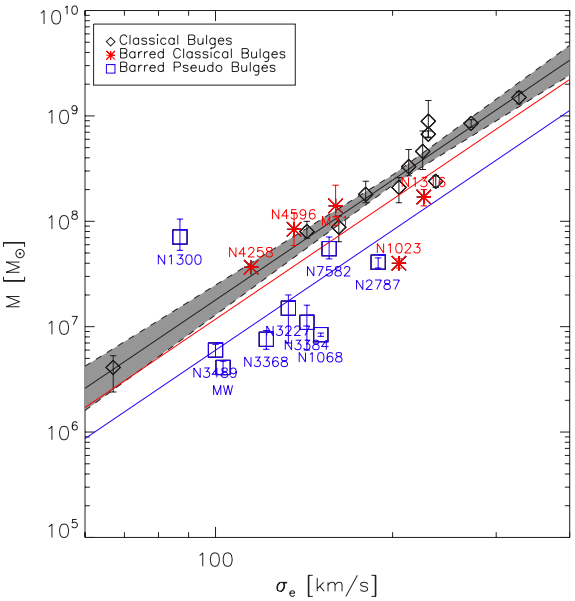

Figure 13. The $M_\bullet - \sigma_e$ relations of classical bulges in unbarred galaxies, and of classical- and pseudo-bulges in barred galaxies from Table 4. The solid black line shows the linear regression of the unbarred classical bulges, while the shaded region bounded by the dashed black lines shows the one σ uncertainty. The solid red and blue lines show fits for the classical- and pseudo-bulges, respectively, in barred galaxies with slope fixed to that for unbarred classical bulges.

scatter of only 0.11 dex, as can be seen in Fig. 13. While this can merely be due to small number statistics, the wide range of σ_e considered, $67 \leq \sigma_e \leq 328\,\mathrm{km\,s^{-1}}$, hints that our approach of selecting sub-samples based on bulge type is reasonable.

The fit we obtain for unbarred classical bulges is in fairly good agreement with the fit to elliptical galaxies (excluding brightest cluster galaxies) of Debattista et al. (2013): $(\alpha, \beta) = (8.21 \pm 0.07, 4.06 \pm 0.40)$. If we fix $\beta = 4.06$ and refit these 12 unbarred galaxies with classical bulges, we obtain $\alpha = 8.41 \pm 0.05$, which confirms the lack of an offset between ellipticals and unbarred classical bulges. Debattista et al. (2013) used this result to argue for the need of SMBHs in classical bulges to grow along with the discs.

5.3 The $M_\bullet - \sigma_e$ relations of barred galaxies

We then fix $\beta = 3.78$, the value we obtained for unbarred classical bulges, and fit the $M_\bullet - \sigma_e$ relation of barred galaxies with classical bulges. We obtain $(\alpha, \epsilon_0) = (8.21 \pm 0.19, 0.41)$, or $\delta\alpha = -0.18 \pm 0.20$ dex. This offset, which is visible in Fig. 13, is smaller than the $\delta\alpha = -0.5$ dex found by Graham et al. (2011) (who however considered all barred galaxies, not just those with classical bulges). The offset we find is consistent with the one predicted by the models (see Table 3). However, with this small sample it is also consistent with no offset. The offset is largely driven by NGC 1023, while NGC 1316 also falls below the unbarred $M_\bullet - \sigma_e$ relation. Therefore, the main limitation of our comparison to observations is the small sample size for barred classical bulges. The observed scatter in the $M_\bullet - \sigma_e$ relation of barred classical bulges is more than twice as large as that predicted by adding in quadrature the intrinsic scatter of unbarred classical bulges (0.11) to the scatter induced by bars in our models (0.16). The main reason for this discrepancy is very likely the narrow range of models we have considered, which reduces the predicted scatter. Moreover, if some SMBHs in barred galaxies are able to grow again, returning to the fiducial $M_\bullet - \sigma_e$ relation, then this would further increase the scatter relative to the offset relation. Indeed, M31, NGC 4258 and NGC 4596 are all close to the $M_\bullet - \sigma_e$ relation of unbarred classical bulges. Of these, M31 and NGC 4258 both have gas. NGC 4258 is also the only galaxy in this sample with a weak bar. Finally, the observed scatter for barred galaxies may be enhanced by modelling uncertainties. For instance, in the presence of a bar, the growth of an SMBH results in a larger increase in σ_e than it would in an axisymmetric galaxy. However, the kinematics of stars associated with the bar results in a smaller and frequently negative Gauss–Hermite coefficient h_4. Brown et al. (2013) argue that using an axisymmetric stellar dynamical modelling to measure SMBH masses in barred galaxies could result in an overestimate of the derived $M_\bullet$ since low/negative h_4 values primarily result from a large fraction of stars on tangential orbits, which in turn requires a larger enclosed mass to fit the large velocity dispersion.

The fit for the pseudo-bulge barred sample gives $(\alpha, \epsilon_0) = (7.91 \pm 0.18, 0.50)$. The offset, also seen in Fig. 13, is $\delta\alpha = -0.48 \pm 0.19$ dex, which is considerably larger than in the simulations. It is unclear whether compression of the bulge by bar evolution is the main cause for the offset in the case of pseudo-bulges. The Milky Way, which has a bar and which we have classified as having a pseudo-bulge, is right in the middle of the $M_\bullet - \sigma_e$ relation of barred galaxies with pseudo-bulges.

6 DISCUSSION AND CONCLUSIONS

6.1 Offset and scatter in the $M_\bullet - \sigma_e$ relation

We have studied the consequences of angular momentum redistribution driven by bars on the evolution of the velocity dispersion, σ_e, of the bulge and the implications for the $M_\bullet - \sigma_e$ relation. We showed that if $M_\bullet$ does not grow during the formation and evolution of bars, then the increase in σ_e results in an offset below the $M_\bullet - \sigma_e$ relation. The simulations predict an offset $\delta\alpha \sim -0.2$.

Defining a sample of observed classical bulges from the literature, we fit the $M_\bullet - \sigma_e$ relation of unbarred galaxies. Then, fixing the slope of the relation, we fit the relation for the classical bulges in barred galaxies, and find an offset from the unbarred galaxies of $\delta\alpha = -0.18 \pm 0.20$, consistent with the prediction but also consistent with no offset.

Contamination of the bulge velocity dispersion by the kinematics of the disc can lead to changes in σ_e by as much as 25 per cent, equivalent to an offset in the $M_\bullet - \sigma_e$ relation as large as $\delta\alpha \sim -0.4$ (for $\beta = 4$). However, this contamination should also be present in

the sample of unbarred galaxies relative to which we measure the offset for the barred galaxies. Thus, contamination by the disc is very unlikely to cause an offset.

The models imply that the scatter should increase (in quadrature) by ∼0.16; we measure a scatter for unbarred galaxies of 0.11 and for barred classical bulges of 0.41. This is larger than the predicted scatter, but our prediction is based on a narrow range of models and does not take into account the possibility that SMBHs can grow back on to the $M_\bullet - \sigma_e$ relation, both of which would increase the scatter. In addition, our models cover only a narrow range of bulge-to-disc ratios. Moreover, the dynamical measurements of $M_\bullet$ probably include systematic errors that arise from modelling barred galaxies as axisymmetric galaxies (Brown et al. 2013), adding to the scatter in the $M_\bullet - \sigma_e$ relationship.

6.2 The black hole Fundamental Plane

Several studies have suggested that departures from the $M_\bullet - \sigma_e$ relation correlate with a third, structural, parameter, such as $R_{\rm eff}$ or the stellar mass of the bulge $M_{\rm bul}$ (Marconi & Hunt 2003; de Francesco, Capetti & Marconi 2006; Aller & Richstone 2007; Barway & Kembhavi 2007; Hopkins et al. 2007a). This has come to be known as the black hole Fundamental Plane (BHFP), and both its existence and origin have been a subject of uncertainty. This is because the BHFP, if it exists, is strongly dominated by σ_e (e.g. Beifiori et al. 2012). Hopkins et al. (2007b) proposed that the BHFP may arise from the higher gas mass fraction of merger progenitors at high redshift. Graham (2008a) instead argued that barred galaxies may wholly account for the BHFP, given the current data. We have shown that the residuals in the $M_\bullet - \sigma_e$ relation caused by bar evolution correlate with structural and kinematic properties of the system. In the former case, this can account for the weak BHFP measured thus far. For the models, we find a strong correlation between $\delta \log \mathrm{M}_\bullet$ and $M(B)/M(B+D)$; observationally however, the BHFP is much weaker, and this perhaps reflects the fact that the models we have considered here have a relatively narrow range of B/D initially, leading to a strong correlation between $M(B)/M(B+D)$ and $\Delta M(B+D)/M(B+D)_{\rm init}$. A wider range of initial bulge-to-disc ratios is likely to blur the correlation between $M(B)/M(B+D)$ and $\Delta M(B+D)/M(B+D)_{\rm init}$, making for a weaker structural BHFP. In addition, we are able to fully disentangle bulges from discs in the simulations, allowing us to compute $M(B)/M(B+D)$. Observationally, disentangling the bulge mass at small radii, where the disc profile may no longer follow an inward extrapolation of an exponential profile, may present difficulties.

We have also shown that $\delta \log \mathrm{M}_\bullet$ strongly correlates with $\beta_\phi(B+D)$ and $\beta_z(B+D)$, which potentially present new versions of the BHFP where the third parameter is a kinematic one. This correlation is unlikely to be as sensitive to a wider range of initial conditions, but this still needs to be tested further.

6.3 The role of gas

Using *HST* Space Telescope Imaging Spectrograph spectra to measure upper limits on $M_\bullet$ in 105 low-luminosity AGN, Beifiori et al. (2009) found no offset between the $M_\bullet - \sigma_e$ relations of barred and unbarred galaxies. Likewise, in a study of 76 active galaxies, Xiao et al. (2011) also found no difference between barred and unbarred galaxies. The main difference between these observations and our results is the presence of gas. The simulations presented here are all collisionless. As the bar grows, σ_e increases and SMBHs fall below the $M_\bullet - \sigma_e$ relation. This offset can be reversed if the SMBH can grow, which they can best do by accreting gas. It is now clear that low-to-medium luminosity AGN are overwhelmingly resident in disc galaxies. Thus, secular processes in disc galaxies must play an important role in the growth of SMBHs (Cisternas et al. 2011; Schawinski et al. 2011, 2012; Araya Salvo et al. 2012; Kocevski et al. 2012; Simmons et al. 2012; Treister et al. 2012; Debattista et al. 2013). It seems likely that, after a bar forms, an SMBH will drop below the $M_\bullet - \sigma_e$ relation, but, once gas is driven to the centre, the SMBH can grow again. If SMBH growth is governed by AGN feedback, then it would be able to return to the $M_\bullet - \sigma_e$ relation. This path to returning to the $M_\bullet - \sigma_e$ relation is however not available to galaxies without gas to trickle down to the SMBH. The fact that galaxy samples with ongoing AGN activity, such as those of Beifiori et al. (2009) and Xiao et al. (2011), do not show an offset suggests that bars are efficient at feeding SMBHs.

6.4 Future observational prospects

The sample of observed barred galaxies with classical bulges we have used here includes just five galaxies. The most immediate way of extending our results will come from careful bulge classification of the remaining barred sample. We explored what would happen if the sample of unclassified bulge barred galaxies in Table 4 all hosted classical bulges, which is very unlikely but gives us an indication of how the offset is likely to vary. Fitting the $M_\bullet - \sigma_e$ relation with $\beta = 3.78$ gives a larger offset $\delta\alpha = -0.50 \pm 0.14$ (see Table 5 for full fit). Curiously, other than NGC 4151, all the rest of these galaxies are either on (within the error) or offset below the $M_\bullet - \sigma_e$ relation, suggesting that a large offset is likely. Thus, the presence of an offset between unbarred and barred galaxies with classical bulges may get stronger.

6.5 Caveats

Two important caveats need to be borne in mind about our results. First of all the models considered in this paper have been drawn from a probability distribution appropriate for properties of the Milky Way. At best only one of these models is an accurate representation of the Milky Way. It is unlikely that a distribution of models of a single galaxy is a reasonable representation of the intrinsic variety of galaxies in general, even at fixed galaxy mass. For example, the bulge-to-disc ratio in the models takes on a narrow range of values $0.15 \leq B/D \leq 0.28$, whereas the barred sample in Table 4 has an order of magnitude larger variation in B/D. This may bias the values of the offset in the $M_\bullet - \sigma_e$ relation to larger values while decreasing the scatter of the models.

In addition, all the models as constructed are already bar unstable from the start. We note in particular that about half the models have a minimum Toomre-Q between 1.0 and 1.5. Thus, many of the models need to shed a significant amount of angular momentum in order to form a bar. Whether nature forms disc galaxies that are this unstable is unclear; for instance the high-resolution models of Roškar et al. (2012), in which the stars all formed out of cooling gas, rather than put in ab initio as here, tend to evolve at constant Q slightly lower than 2. Indeed, the values in Table 2 show that smaller values of minimum Q produce larger values of $\langle \sigma_{\rm e}/\sigma_{e0} \rangle$. We note that the correlation of Q with $\langle \sigma_{\rm e}/\sigma_{e0} \rangle$ ($r_{\rm s} = -0.57$) is stronger than with $A_{\rm bar}$ ($r_{\rm s} = 0.19$) or with $\Delta M/M_{\rm init}$ ($r_{\rm s} = -0.44$). Thus, these models may shed more angular momentum from the disc centre than in nature, leading to a larger increase in the disc mass at the centre, a larger increase in σ_e and thus a larger offset in the $M_\bullet - \sigma_e$ relation.

6.6 Summary

We have studied the consequences of bar formation and evolution on the $M_\bullet - \sigma_e$ relation of SMBHs. Our main results can be summarized as follows.

(i) Models show that bars cause an increase in the central mass density of a galaxy, altering the kinematics of the bulge and of the disc. Of particular importance for the $M_\bullet - \sigma_e$ relation is the increase in σ_e. We find a strong correlation between the ratio of final to initial dispersion, $\langle \sigma_e / \sigma_{e0} \rangle$, and the fractional change in mass of the bulge+disc within $R_{\rm eff}$ of the bulge, in good agreement with Debattista et al. (2013). The simulations show that $\sigma_e(B)$ can increase by as much $\sim$20 per cent for a slope $\beta = 4$. An SMBH in such a galaxy would need to grow by a factor of $\sim$2 to remain on the $M_\bullet - \sigma_e$ relation. The average fractional increase of $\sigma_e(B)$ in the simulations is $\langle \sigma_e / \sigma_{e0} \rangle = 1.12 \pm 0.05$.

(ii) The simulations show that while $\sigma(B + D)$ correlates with $\sigma(B)$, the two are not equal; thus, the disc contaminates the measurement of the bulge velocity dispersion. In the edge-on view, $\sigma_e(B + D)$ and $\sigma_{e/8}(B + D)$ are up to 25 per cent larger than $\sigma_e(B)$ and $\sigma_{e/8}(B)$. $\sigma_{e/8}(B + D)/\sigma_{e/8}(B)$ and $\sigma_e(B + D)/\sigma_e(B)$ follow the same distribution, but the scatter in $\sigma_{e/8}(B + D)$ is slightly larger than the scatter in $\sigma_e(B + D)$. Thus, σ_e is a better quantity for studying SMBH scaling relations.

(iii) We use the $M_\bullet - \sigma_e$ relation of Gültekin et al. (2009) and the models to estimate the offset of barred galaxies in the absence of SMBH growth. We predict an offset $\delta\alpha \sim -0.2$ for a slope of $\beta = 4$ and an increase in quadrature of the scatter by $\epsilon_0 \sim 0.16$.

(iv) We showed that the tangential anisotropy, $\beta_\phi(B + D)$ correlates very strongly with the change in mass within $R_{\rm eff}$. Since this in turn correlates with the change in σ_e, this suggests that residuals of galaxies from the $M_\bullet - \sigma_e$ relation may also correlate very strongly with $\beta_\phi(B + D)$, which is the case for the simulations. This may provide a new version of the BHFP, where the third parameter is a kinematic one.

(v) From published samples of observed galaxies, we obtain a sample of twelve galaxies to measure the $M_\bullet - \sigma_e$ relation of unbarred disc galaxies with classical bulges. We find $(\alpha, \beta) = (8.39 \pm 0.05, 3.78 \pm 0.31)$. Then, fixing the slope β, we fit the $M_\bullet - \sigma_e$ relation for five barred galaxies with classical bulges. We find $\delta\alpha = -0.18 \pm 0.20$, comparable to the prediction from the models but also consistent with no offset. The same exercise for nine pseudo-bulges in barred galaxies yields an offset $\delta\alpha = -0.48 \pm 0.19$. The scatter in the $M_\bullet - \sigma_e$ relation of the barred classical bulges is larger than the one for unbarred classical-bulged galaxies by an amount larger than predicted. This may be because the scatter in the models underestimates the real scatter and because SMBHs in barred galaxies are able to grow again, returning to the fiducial $M_\bullet - \sigma_e$ relation. SMBH mass measurements in barred galaxies may also be more uncertain than in unbarred galaxies (Brown et al. 2013).

ACKNOWLEDGEMENTS

We thank Helen Cammack, Samuel Heald and especially Lindsey Tate, who worked on parts of the analysis of these simulations during summer internships. We thank the Nuffield Foundation for supporting Samuel Heald via a Nuffield Internship during the summer of 2010. Markus Hartmann thanks Kayan Gueltekin and Alessandra Beifiori for helpful discussion. We also thank John Dubinski for sharing with us the carefully constructed simulations used in this paper. We acknowledge Peter Erwin for alerting us to the fact that literature compilations of $M_\bullet - \sigma_e$ measurements contain a wrong value for the velocity dispersion of NGC 1300. We thank the anonymous referee for a constructive report. VPD and DRC are supported by STFC Consolidated grant ST/J001341/1. MV is supported by US National Science Foundation grant AST-0908346. LMW was supported by a Discovery Grant with the Natural Sciences and Engineering Research Council of Canada. The final stages of this work were supported by the National Science Foundation under Grant no. PHY-1066293 and the hospitality of the Aspen Center for Physics.

REFERENCES

Adams F. C., Graff D. S., Richstone D. O., 2001, ApJ, 551, L31
Adams F. C., Graff D. S., Mbonye M., Richstone D. O., 2003, ApJ, 591, 125
Aller M. C., Richstone D. O., 2007, ApJ, 665, 120
Araki S., 1987, AJ, 94, 99
Araya Salvo C., Mathur S., Ghosh H., Fiore F., Ferrarese L., 2012, ApJ, 757, 179
Athanassoula E., 1992, MNRAS, 259, 345
Athanassoula E., 2002, ApJ, 569, L83
Athanassoula E., 2003, MNRAS, 341, 1179
Athanassoula E., 2005, MNRAS, 358, 1477
Athanassoula E., Beaton R. L., 2006, MNRAS, 370, 1499
Baes M., Buyle P., Hau G. K. T., Dejonghe H., 2003, MNRAS, 341, L44
Barway S., Kembhavi A., 2007, ApJ, 662, L67
Batcheldor D. et al., 2005, ApJS, 160, 76
Baugh C. M., Cole S., Frenk C. S., 1996, MNRAS, 283, 1361
Beifiori A., Sarzi M., Corsini E. M., Dalla Bontà E., Pizzella A., Coccato L., Bertola F., 2009, ApJ, 692, 856
Beifiori A., Courteau S., Corsini E. M., Zhu Y., 2012, MNRAS, 419, 2497
Beletsky Y., Gadotti D. A., Moiseev A., Alves J., Kniazev A., 2011, MNRAS, 418, L6
Bender R., Burstein D., Faber S. M., 1992, ApJ, 399, 462
Berentzen I., Shlosman I., Martinez-Valpuesta I., Heller C. H., 2007, ApJ, 666, 189
Berrier J. C. et al., 2013, ApJ, 769, 132
Binney J., Tremaine S., 2008, Galactic Dynamics, 2nd edn. Princeton Univ. Press, Princeton, NJ
Bissantz N., Gerhard O., 2002, MNRAS, 330, 591
Booth C. M., Schaye J., 2009, MNRAS, 398, 53
Brown J. S., Valluri M., Shen J., Debattista V. P., 2013, ApJ, 778, 151
Bureau M., Athanassoula E., 1999, ApJ, 522, 686
Burkert A., Tremaine S., 2010, ApJ, 720, 516
Cid Fernandes R., Gu Q., Melnick J., Terlevich E., Terlevich R., Kunth D., Rodrigues Lacerda R., Joguet B., 2004, MNRAS, 355, 273
Cisternas M. et al., 2011, ApJ, 726, 57
Cisternas M. et al., 2013, ApJ, 776, 50
Combes F., Sanders R. H., 1981, A&A, 96, 164
Combes F., Debbasch F., Friedli D., Pfenniger D., 1990, A&A, 233, 82
Courteau S., de Jong R. S., Broeils A. H., 1996, ApJ, 457, L73
Davies R. L., Illingworth G., 1983, ApJ, 266, 516
de Francesco G., Capetti A., Marconi A., 2006, A&A, 460, 439
Debattista V. P., Sellwood J. A., 2000, ApJ, 543, 704
Debattista V. P., Carollo C. M., Mayer L., Moore B., 2004, ApJ, 604, L93
Debattista V. P., Carollo C. M., Mayer L., Moore B., 2005, ApJ, 628, 678
Debattista V. P., Mayer L., Carollo C. M., Moore B., Wadsley J., Quinn T., 2006, ApJ, 645, 209
Debattista V. P., Kazantzidis S., van den Bosch F. C., 2013, ApJ, 765, 23
Di Matteo T., Springel V., Hernquist L., 2005, Nature, 433, 604
Drory N., Fisher D. B., 2007, ApJ, 664, 640
Dubinski J., 1996, New Astron., 1, 133
Eggen O. J., Sandage A. R., 1962, ApJ, 136, 735
Elmegreen B. G., Elmegreen D. M., Hirst A. C., 2004, ApJ, 612, 191

Eskridge P. B. et al., 2000, AJ, 119, 536
Fabricius M. H., Saglia R. P., Fisher D. B., Drory N., Bender R., Hopp U., 2012, ApJ, 754, 67
Ferrarese L., 2002, ApJ, 578, 90
Ferrarese L., Ford H., 2005, Space Sci. Rev., 116, 523
Ferrarese L., Merritt D., 2000, ApJ, 539, L9
Fisher D. B., Drory N., 2008, AJ, 136, 773
Fisher D. B., Drory N., 2010, ApJ, 716, 942
Fisher D. B., Drory N., 2011, ApJ, 733, L47
Gadotti D. A., 2009, MNRAS, 393, 1531
Gadotti D. A., Kauffmann G., 2009, MNRAS, 399, 621
Gebhardt K. et al., 2000, ApJ, 539, L13
Gebhardt K. et al., 2003, ApJ, 583, 92
Goldreich P., Tremaine S., 1978, ApJ, 222, 850
Goldreich P., Tremaine S., 1979, ApJ, 233, 857
Graham A. W., 2007, MNRAS, 379, 711
Graham A. W., 2008a, PASA, 25, 167
Graham A. W., 2008b, ApJ, 680, 143
Graham A. W., 2012, ApJ, 746, 113
Graham A. W., Driver S. P., 2007, MNRAS, 380, L15
Graham A. W., Li I., 2009, ApJ, 698, 812
Graham A. W., Scott N., 2013, ApJ, 764, 151
Graham A. W., Erwin P., Caon N., Trujillo I., 2001, ApJ, 563, L11
Graham A. W., Onken C. A., Athanassoula E., Combes F., 2011, MNRAS, 412, 2211
Gültekin K. et al., 2009, ApJ, 698, 198
Häring N., Rix H., 2004, ApJ, 604, L89
Harris G. L. H., Harris W. E., 2011, MNRAS, 410, 2347
Hicks E. K. S., Davies R. I., Maciejewski W., Emsellem E., Malkan M. A., Dumas G., Müller-Sánchez F., Rivers A., 2013, ApJ, 768, 107
Hirschmann M., Khochfar S., Burkert A., Naab T., Genel S., Somerville R. S., 2010, MNRAS, 407, 1016
Hohl F., 1971, ApJ, 168, 343
Hopkins P. F., Hernquist L., Cox T. J., Robertson B., Krause E., 2007a, ApJ, 669, 45
Hopkins P. F., Hernquist L., Cox T. J., Robertson B., Krause E., 2007b, ApJ, 669, 67
Hu J., 2008, MNRAS, 386, 2242
Jahnke K., Macciò A. V., 2011, ApJ, 734, 92
Jogee S. et al., 2004, ApJ, 615, L105
Jogee S., Scoville N., Kenney J. D. P., 2005, ApJ, 630, 837
Kauffmann G., White S. D. M., Guiderdoni B., 1993, MNRAS, 264, 201
King A., 2003, ApJ, 596, L27
Knapen J. H., 1999, in Beckman J. E., Mahoney T. J., eds, ASP Conf. Ser. Vol. 187, The Evolution of Galaxies on Cosmological Timescales. Astron. Soc. Pac, San Francisco, p. 72
Kocevski D. D. et al., 2012, ApJ, 744, 148
Kormendy J., Bender R., 2009, ApJ, 691, L142
Kormendy J., Bender R., 2011, Nature, 469, 377
Kormendy J., Illingworth G., 1982, ApJ, 256, 460
Kormendy J., Kennicutt R. C., Jr, 2004, ARA&A, 42, 603
Kormendy J., Richstone D., 1995, ARA&A, 33, 581
Kormendy J., Bender R., Cornell M. E., 2011, Nature, 469, 374
Krajnović D. et al., 2013, MNRAS, 432, 1768
Kuijken K., Dubinski J., 1995, MNRAS, 277, 1341
Lauer T. R. et al., 2007, ApJ, 662, 808
Lynden-Bell D., Kalnajs A. J., 1972, MNRAS, 157, 1
McConnell N. J., Ma C.-P., 2013, ApJ, 764, 184
McConnell N. J., Ma C.-P., Gebhardt K., Wright S. A., Murphy J. D., Lauer T. R., Graham J. R., Richstone D. O., 2011, Nature, 480, 215
McLeod K. K., Rieke G. H., 1995, ApJ, 441, 96
McLure R. J., Dunlop J. S., 2002, MNRAS, 331, 795
Magorrian J. et al., 1998, AJ, 115, 2285
Marconi A., Hunt L. K., 2003, ApJ, 589, L21
Markwardt C. B., 2009, in Bohlender D. A., Durand D., Dowler P., eds, ASP Conf. Ser. Vol. 411, Astronomical Data Analysis Software and Systems XVIII. Astron. Soc. Pac., San Francisco, p. 251
Masters K. L. et al., 2011, MNRAS, 411, 2026
Merritt D., Ferrarese L., 2001, ApJ, 547, 140
Merritt D., Sellwood J. A., 1994, ApJ, 425, 551
Mulchaey J. S., Regan M. W., 1997, ApJ, 482, L135
Murray N., Quataert E., Thompson T. A., 2005, ApJ, 618, 569
Naab T., Johansson P. H., Ostriker J. P., Efstathiou G., 2007, ApJ, 658, 710
Nair P. B., Abraham R. G., 2010, ApJ, 714, L260
Norman C. A., Sellwood J. A., Hasan H., 1996, ApJ, 462, 114
Paturel G., Petit C., Prugniel P., Theureau G., Rousseau J., Brouty M., Dubois P., Cambrésy L., 2003, A&A, 412, 45
Peng C. Y., 2007, ApJ, 671, 1098
Pota V., Graham A. W., Forbes D. A., Romanowsky A. J., Brodie J. P., Strader J., 2013, MNRAS, 433, 235
Power C., Zubovas K., Nayakshin S., King A. R., 2011, MNRAS, 413, L110
Prugniel P., Simien F., 1997, A&A, 321, 111
Raha N., Sellwood J. A., James R. A., Kahn F. D., 1991, Nature, 352, 411
Rhode K. L., 2012, AJ, 144, 154
Roškar R., Debattista V. P., Quinn T. R., Wadsley J., 2012, MNRAS, 426, 2089
Rusli S. P., Thomas J., Erwin P., Saglia R. P., Nowak N., Bender R., 2011, MNRAS, 410, 1223
Sadoun R., Colin J., 2012, MNRAS, 426, L51
Saha K., Martinez-Valpuesta I., Gerhard O., 2012, MNRAS, 421, 333
Sani E., Marconi A., Hunt L. K., Risaliti G., 2011, MNRAS, 413, 1479
Sazonov S. Y., Ostriker J. P., Ciotti L., Sunyaev R. A., 2005, MNRAS, 358, 168
Schawinski K., Treister E., Urry C. M., Cardamone C. N., Simmons B., Yi S. K., 2011, ApJ, 727, L31
Schawinski K., Simmons B. D., Urry C. M., Treister E., Glikman E., 2012, MNRAS, 425, L61
Searle L., Zinn R., 1978, ApJ, 225, 357
Seigar M. S., Kennefick D., Kennefick J., Lacy C. H. S., 2008, ApJ, 678, L93
Sellwood J. A., 2006, ApJ, 637, 567
Sellwood J. A., Debattista V. P., 2009, MNRAS, 398, 1279
Shabala S. S., Ash S., Alexander P., Riley J. M., 2008, MNRAS, 388, 625
Shankar F., Marulli F., Mathur S., Bernardi M., Bournaud F., 2012, A&A, 540, A23
Sheth K. et al., 2008, ApJ, 675, 1141
Shlosman I., Frank J., Begelman M. C., 1989, Nature, 338, 45
Silk J., Rees M. J., 1998, A&A, 331, L1
Simkin S. M., Su H. J., Schwarz M. P., 1980, ApJ, 237, 404
Simmons B. D., Urry C. M., Schawinski K., Cardamone C., Glikman E., 2012, ApJ, 761, 75
Skibba R. A. et al., 2012, MNRAS, 423, 1485
Terzić B., Graham A. W., 2005, MNRAS, 362, 197
Toomre A., 1964, ApJ, 139, 1217
Toomre A., 1981, in Fall S. M., Lynden-Bell D., eds, Structure and Evolution of Normal Galaxies. Cambridge Univ. Press, Cambridge, p. 111
Treister E., Schawinski K., Urry C. M., Simmons B. D., 2012, ApJ, 758, L39
Tremaine S., Weinberg M. D., 1984, MNRAS, 209, 729
Tremaine S. D., Ostriker J. P., Spitzer L., Jr, 1975, ApJ, 196, 407
Tremaine S. et al., 2002, ApJ, 574, 740
van den Bosch F. C., 1998, ApJ, 507, 601
Volonteri M., Natarajan P., 2009, MNRAS, 400, 1911
Volonteri M., Natarajan P., Gültekin K., 2011, ApJ, 737, 50
Widrow L. M., Dubinski J., 2005, ApJ, 631, 838
Widrow L. M., Pym B., Dubinski J., 2008, ApJ, 679, 1239 (W08)
Wyithe J. S. B., Loeb A., 2003, ApJ, 595, 614
Wyse R. F. G., Gilmore G., Franx M., 1997, ARA&A, 35, 637
Xiao T., Barth A. J., Greene J. E., Ho L. C., Bentz M. C., Ludwig R. R., Jiang Y., 2011, ApJ, 739, 28
Younger J. D., Hopkins P. F., Cox T. J., Hernquist L., 2008, ApJ, 686, 815

This paper has been typeset from a TEX/LATEX file prepared by the author.